minerals

MDPI

Article

LA-ICP-MS Trace Element Geochemistry of Sphalerite and Metallogenic Constraints: A Case Study from Nanmushu Zn–Pb Deposit in the Mayuan District, Shaanxi Province, China

Junjie Wu [1,2], Huixin Dai [1,*], Yong Cheng [3,4,*], Saihua Xu [1,*], Qi Nie [3], Yiming Wen [3] and Ping Lu [3]

1 Faculty of Land and Resource Engineering, Kunming University of Science and Technology, Kunming 650093, China; starwjj555@126.com
2 Shaanxi Institute of Geology and Mineral Resources Experiment Co., Ltd., Xi'an 710054, China
3 Faculty of Metallurgy and Mining Engineering, Kunming Metallurgy College, Kunming 650033, China; kiki158961326@163.com (Q.N.); kmcymw@163.com (Y.W.); lupingin@163.com (P.L.)
4 School of Earth Sciences, Yunnan University, Kunming 650500, China
* Correspondence: dhxk_must@163.com (H.D.); cheng_yong1988@163.com (Y.C.); xusaihua18@126.com (S.X.)

Abstract: The Nanmushu Zn–Pb deposit is a large-scale and representative deposit in the Mayuan ore field on the northern margin of the Yangtze Block. This study investigates the trace element geochemistry of sphalerite from this deposit using laser ablation inductively coupled plasma mass spectrometry (LA-ICP-MS). The results show that the main trace elements in sphalerite include various trace elements, such as Mn, Fe, Cu, Ga, Ge, Ag, Cd, Pb, Co, Hg, Tl, In, Sn, and Sb. Among them, Ag, Ge, Cd, and Cu are valuable components that may be recovered during mineral processing or smelting techniques. The histograms, LA-ICP-MS time-resolved depth profiles, and linear scan profiles indicated that most trace elements occur in sphalerite as isomorphs, while partial Pb, Fe, and Ag occur as tiny mineral inclusions. The correlation diagrams of trace elements revealed that Fe^{2+}, Mn^{2+}, Pb^{2+}, and Tl^{3+} can substitute Zn^{2+} in sphalerite through isomorphism. In sphalerite, Cd^{2+} and Hg^{2+} together or Mn^{2+}, Pb^{2+}, and Tl^{3+} together can replace Zn^{2+}, i.e., $((3Mn, 3Pb, 2Tl)^{6+}, 3(Cd, Hg)^{2+}) \leftrightarrow 3Zn^{2+}$. Moreover, there is a mechanism of Ge^{4+} with Cu^{+} or Ga^{3+} with Cu_{+} replacing Zn^{2+} in the Nanmushu deposit, i.e., $Ge^{4+} + 2Cu^{+} \leftrightarrow 3Zn^{2+}$ or $2Ga^{3+} + 2Cu^{+} \leftrightarrow 4Zn^{2+}$. Furthermore, the trace element compositions indicate that the Nanmushu Zn mineralization occurred under low-temperature conditions (<200 °C) and should be classified as a Mississippi Valley-type (MVT) deposit. This study provides new insights into the occurrence and substitution mechanisms of trace elements in sphalerite and the metallogenic constraints of the Nanmushu deposit.

Keywords: in-site trace elements; sphalerite; substitution mechanisms; Nanmushu Zn–Pb deposit; Mayuan district; Mississippi Valley-type (MVT) deposit

check for updates

Citation: Wu, J.; Dai, H.; Cheng, Y.; Xu, S.; Nie, Q.; Wen, Y.; Lu, P. LA-ICP-MS Trace Element Geochemistry of Sphalerite and Metallogenic Constraints: A Case Study from Nanmushu Zn–Pb Deposit in the Mayuan District, Shaanxi Province, China. *Minerals* **2023**, *13*, 793. https://doi.org/10.3390/min13060793

Academic Editor: Maria Boni

Received: 9 May 2023
Revised: 1 June 2023
Accepted: 6 June 2023
Published: 10 June 2023

1. Introduction

Sphalerite is the predominant ore mineral of lead–zinc (Pb–Zn) deposits and hosts various trace elements, such as Cd, Ga, Ge, In, and other dispersed elements [1–6]. These elements have diverse applications in many high-tech fields [7]. For instance, Cd alloys serve as bearing materials for aircraft engines and control rods (neutron absorption) for nuclear reactors, and Cd–Ni batteries are essential for aviation and railways [4]. Ga plays a role In new generation information technology, biotechnology, high-end equipment manufacturing, new energy, and new materials [8]. Ge is employed in information communication, modern aviation, modern military, and new energy sectors [9]. In is used in the electronics industry, aerospace, alloy manufacturing, solar cell new materials, and other fields [10,11]. As strategic resources, Ga, Ge, and In are regarded by many countries as "critical metals" for economic development and the national defence industry [12]. Furthermore, trace elements in sphalerite carry valuable metallogenic information. Some elements constrain the

physical and chemical conditions of ore-forming fluids and can provide reliable ore-forming temperature data as well as indicate the origin of ore deposits [1,13,14].

In recent years, significant progress has been made in the exploration of lead and zinc in the northern margin of the Yangtze block, especially the huge resource prospect of the Mayuan zinc and lead (Zn–Pb) ore field, which has attracted wide attention from geologists. The Zn–Pb mineralization belt has a width of 10–200 m at the Mayuan district and extends over 60 km, which can be divided into three Zn–Pb ore zones, including the south, middle, and north ore zones (Figure 1). The Mayuan Zn–Pb ore field contains a metal resource of over 10 Mt Zn (1.05–10.82 wt%) and Pb (0.55–7.54 wt%) which are associated with some beneficial elements, such as Ag (2–35 ppm), Ge (0.002–0.05 wt%), Cd (0.002–0.10 wt%), and Cu (0.03–0.35 wt%) [15,16]. Many studies have been conducted on the Mayuan Zn–Pb ore field, including the geological features of the ore deposit [15,17], the source of ore-forming materials [16,18–20], the ore-forming age [21–23], the relationship between hydrocarbon organic matters and mineralization [21,24–26], etc. Regarding the genesis of the deposit, the initial understanding was that it was an epigenetic medium-low temperature hydrothermal deposit [27] or a syn-sedimentary hydrothermal deposit [28], but later, most scholars agreed that it was a Mississippi Valley-type (MVT) deposit [16,18–23]. However, studies on the associated beneficial elements are still scarce.

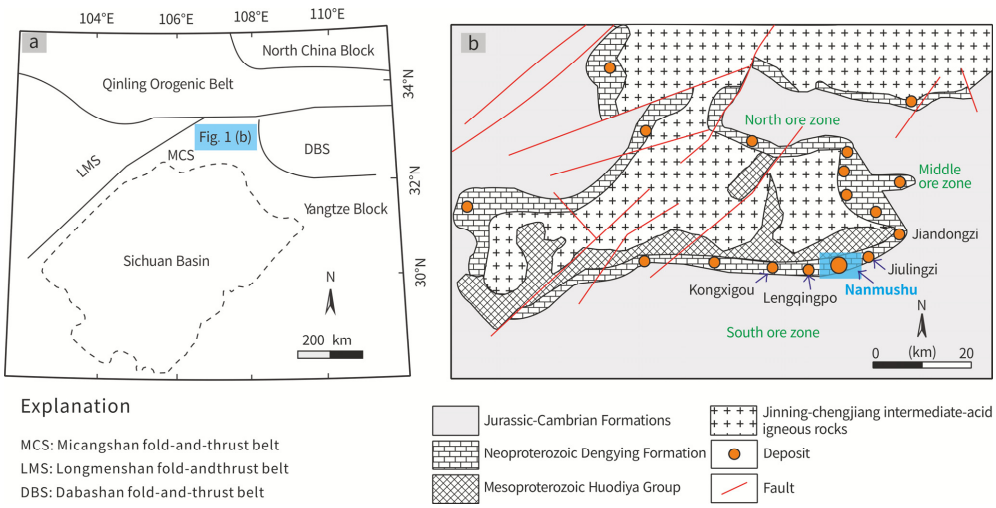

Figure 1. (**a**) Tectonic location of the Mayuan district. (**b**) The distribution of the south, middle, and north ore zones, and major Zn–Pb deposits in the Mayuan district. The figure was modified from reference [20].

The Nanmushu Zn–Pb deposit belongs to the southern ore zone and is the largest deposit in the Mayuan ore field. Previous studies have reported that the associated dispersed elements of the Nanmushu deposit are mainly concentrated in sphalerite [15]. The dissolution method [29] and the in-situ LA-ICP-MS method [19,30,31] show that sphalerite is enriched in the dispersed elements of Cd, Ge, and Ga, while it is relatively depleted in In, Tl, and Se. The occurrence mode and substitution mechanism of major trace elements in sphalerite have not been thoroughly investigated. In this study, the in-situ LA-ICP-MS method was applied to measure the trace elements of sphalerite from the Nanmushu deposit, aiming to discuss the occurrence and substitution mechanism of dispersed elements in sphalerite, estimate and decipher the ore-forming temperature, and provide geochemical constraints on the ore genetic type.

2. Geological Background

2.1. Regional Geology

The study area is located in the south of the Beibadome structure on the northern margin of the Yangtze Block (Figure 1) [20]. The Mayuan district comprises crystalline basement and overlying sedimentary cover. The basement consists of the Huodiya Group

of Mesoproterozoic to Neoproterozoic rocks, and its lithology is mainly meso-deep metamorphic volcaniclastic rocks and magmatic rocks from the Chengjiang to Jinning period, which exhibit angular unconformity with the overlying sedimentary cover. The cover is composed of Sinian–Cambrian shallow metamorphic carbonate rocks and clastic rocks [32].

The regional structure is a large EW-striking Beiba dome structure with pre-Sinian basement in the core and Sinian–Cambrian in the wing [19]. The fault structures in the area are mainly developed along the boundary of basement and caprocks, which are mostly located in caprocks and strike in the same direction as caprocks. In addition, there are also faults formed in a later period obliquely crossing and crosscutting the strata [33].

The Beiba dome structure controls the distribution of ore-bearing strata, and the Pb–Zn ore bodies occur in the brecciform dolostone of the Dengying Formation in a zonal pattern around the dome core [34]. There are three Pb–Zn mineralization zones in the north, east, and south of the study area, and nearly 50 Pb–Zn ore bodies have been discovered, mainly in the south and east ore zones [35]. The most important south ore zone extends in the NEE direction, with a length of more than 30 km and a width of 20–200 m. The average grade of Zn and Pb in the ores is 4.02% and 4.16%, respectively [15]. Kongxigou, Lengqingpo, Nanmushu, Jiulingzi, Jiandongzigou, and other deposits are distributed in this ore zone.

2.2. Ore Deposit Geology

The Nanmushu deposit is one of the most typical deposits in the Mayuan lead–zinc ore field (Figure 2). The exposed strata in the deposit area from old to new are the Mesoproterozoic Huodiya Group, the Upper Sinian Dengying Formation, and the Lower Cambrian Guojiaba Formation [23] (Figure 2). Dengying Formation can be divided into upper and lower lithologic members. The lithology of the lower member is sandstone, including pebbly sandstone with thin layer dolostone. The upper member is dolostone, which can be subdivided into four lithologic beds from bottom to top according to the thickness of the sedimentary layer and rock structure: medium to thick layered dolostone, striated dolostone, brecciform dolostone, and laminar dolostone [20].

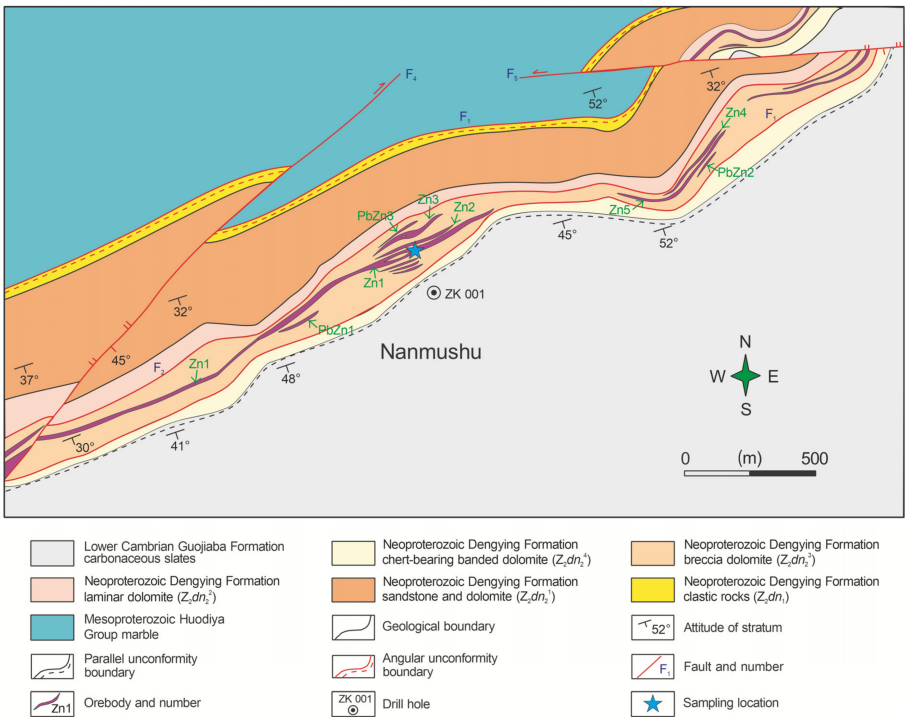

Figure 2. Geological map of the Nanmushu Zn–Pb deposit showing the orebodies are mainly hosted in the third section of Neoproterozoic Dengying Formation breccia dolomite ($Z_2dn_2^3$) (modified from reference [34]).

The ore bodies are stratiform or stratiform-like along the brecciform dolostone of the third lithologic layer of the upper member of the Dengying Formation (Figure 3). Five zinc bodies and three lead–zinc bodies have been discovered in the Nanmu deposit with a length of 100–2560 m and a thickness of 0.80–13.14 m [35]. The deposit contains 2.1 Mt Zn with a grade of 1.05–13.09 wt% and 0.1 Mt Pb with a grade of 0.60–4.12 wt% [21,23].

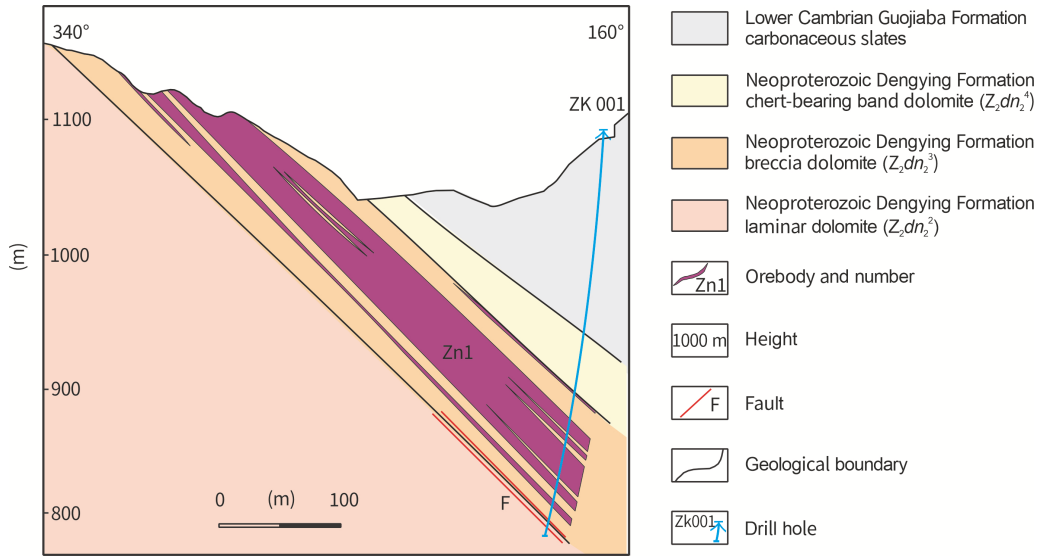

Figure 3. Cross-section of the Nanmushu Zn–Pb deposit (modified from reference [15]).

The ore is dominated by a brecciform structure as well as some stringer disseminated, sparse disseminated, and geode structures. The mineral composition of the ore is relatively simple, and the metal minerals are mainly sphalerite, galena, pyrite, with minor supergene minerals, such as limonite, anglesite, and cerussite. Gangue minerals are mainly dolomite, quartz, bitumen, and minor barite and calcite (Figure 4a–c).

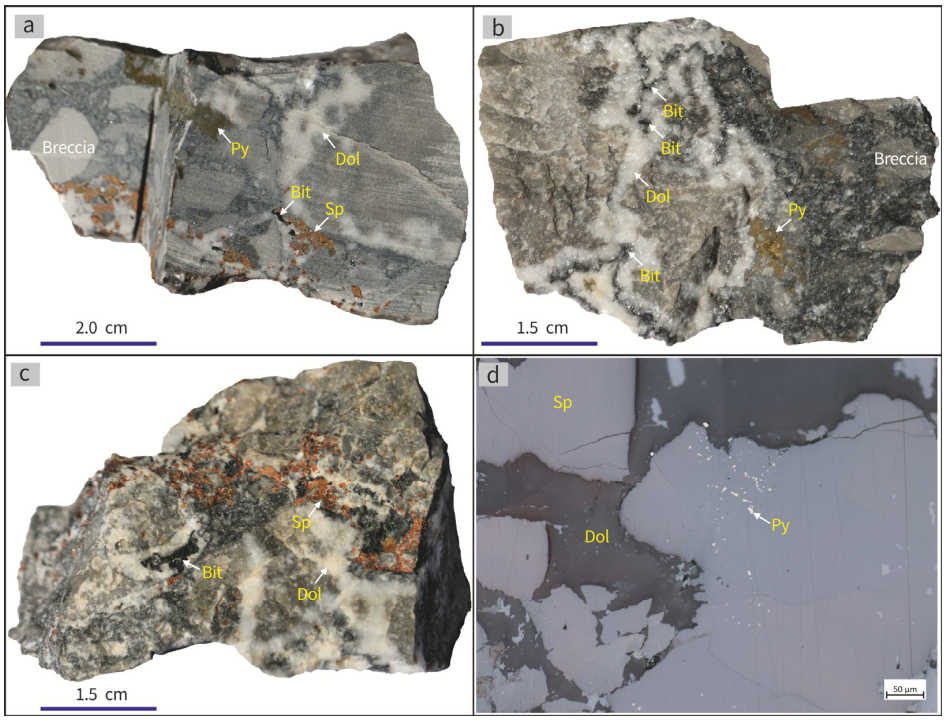

Figure 4. *Cont.*

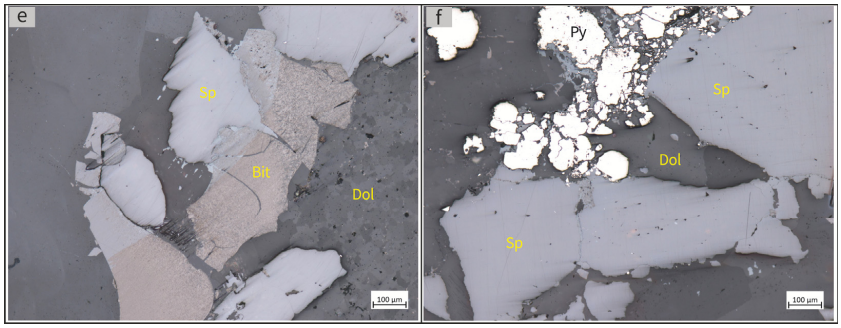

Figure 4. Photographs of the mineralization characteristics of the Nanmushu Zn–Pb deposit. (**a**–**c**) Breccia-type ore. (**a**) Dolostone breccia cemented by later hydrothermal mineral. (**b**) Bitumen is distributed in the dolomite as a thin film or grain, and pyrite is in clumps. (**c**) Sphalerite is associated with bitumen and dolomite. (**d**) Many pyrite inclusions can be seen in the sphalerite particles. (**e**) There are many solid bitumens distributed in the edge of the sphalerite particles. (**f**) Sphalerite is associated with pyrite. Abbreviations: Py = pyrite; Sp = sphalerite; Bit = bitumen; Dol = dolomite.

As the main ore mineral in the ore, sphalerite is mainly distributed in the cement between dolomite breccia, which is tawny or brown, showing glass luster. Microscopically, they are mostly irregular xenomorphic grains with particle sizes ranging from 0.1 mm to 3.0 mm. Sphalerite often has a paragenetic relationship with pyrite and bitumen and is mostly replaced by smithsonite, dolomite, willemite, and hydrozincite (Figure 4e,f). The wall rock alteration of the deposit is weak, mainly involving silicification, carbonatization, pyritization, bituminization, baritization, etc. [26]. According to the geological features and mineral paragenesis relationships of the deposit, it is inferred that the Nanmushu deposit had experienced pre-ore sedimentary and the diagenetic stage, main-ore hydrothermal ore-forming stage, and post-ore supergene stage [22]. In the sedimentary and diagenetic stage, the fine-grained (10 to 50 µm) euhedral pyrite is disseminated within dolomite. A large amount of sphalerite is formed in the hydrothermal stage, which is the economic mineralization stage. Smithsonite, cerussite, and limonite are the main minerals in the post-ore supergene stage [16,20].

3. Samples and Analytical Methods

In this study, samples were collected from the main ore body of the Nanmushu deposit in the Mayuan lead–zinc ore field. Four representative samples were selected to make laser thin sections for testing. Trace elements of sphalerite were determined using a NWR 193 nm ArF Excimer laser ablation system coupled to an iCAP RQ (ICPMS) at Guangzhou Tuoyan Analytical Technology Co., Ltd., Guangzhou, China.

The LA-ICP-MS was tuned using NIST 610 standard glass to yield low oxide production rates. A carrier gas of 0.7 L/min He was fed into the cup, and the aerosol was subsequently mixed with 0.89 L/min Ar make-up gas. The laser fluence was 3.5 J/cm^2, with a repetition rate of 6 Hz, a 30 µm spot size, and an analysis time of 40 s, followed by a 40 s background measurement. The raw isotope data were reduced using the "trace elements" data reduction scheme (DRS). The DRS runs within the freeware IOLITE package of Paton et al. (2011) [36]. In IOLITE, user-defined time intervals are established for the baseline correction procedure to calculate session-wide baseline-corrected values for each isotope. Blocks of two standards (one NIST 610 and one GSE-2G) and one MASS-1 sulfide standard analyses were followed by five to eight unknown samples. For sphalerite, the following 18 isotopes were measured (with their respective dwell times in milliseconds listed in parentheses): ^{34}S, ^{55}Mn, ^{57}Fe, ^{59}Co, ^{60}Ni, ^{65}Cu, ^{66}Zn, ^{71}Ga, ^{74}Ge, ^{75}As, ^{77}Se, ^{107}Ag, ^{111}Cd, ^{118}Sn, ^{121}Sb, ^{126}Hg, ^{205}Tl, and ^{208}Pb, corresponding to a total dwell time of 180 ms. The MASS-1 sulfide standard [37] was used as the primary standard for calibrating ^{34}S, ^{55}Mn, ^{57}Fe,^{59}Co, ^{60}Ni, ^{65}Cu, ^{66}Zn, ^{71}Ga,^{74}Ge,^{75}As, ^{77}Se, ^{107}Ag, ^{111}Cd, ^{118}Sn, ^{121}Sb,

^{126}Hg, ^{205}Tl, and ^{208}Pb. All the isotopes were corrected with an internal standard of ^{66}Zn (Zn = 65).

In addition, three sphalerite particles were selected for line scanning of trace elements. The laser spot size was 10 μm with a scanning speed of 5 μm/S. The other test parameters were the same as above.

4. Results

In this study, a total of 42 LA-ICP-MS spots analyses were completed on 4 sphalerite samples, and the results are listed in Table 1. It can be seen that the trace elements of sphalerite formed in the main mineralization stage of the Nanmushu deposit are mainly Mn, Fe, Cu, Ga, Ge, Ag, Cd, Pb, Co, Hg, Tl, In, Sn, and Sb, while the enrichment degree of other elements is not significant (Figure 5). Furthermore, LA-ICP-MS linear scanning was performed for three sphalerite particles. The complete linear scanning results are shown in Figure 6.

Table 1. LA-ICP-MS in-situ analysis of trace elements of sphalerite in the Nanmushu deposit (ppm).

Sample ID	Spot No.	Mn	Fe	Cu	Ga	Ge	Ag	Cd	Pb	Co	Hg	Tl	In	Sn	Sb
NMS-2 $n = 10$	NMS-2-1	BLD	1531.93	5191.82	85.95	2024.89	41.82	1008.99	23.59	2.84	51.37	0.03	2.85	4.72	1.96
	NMS-2-2	3.96	2321.67	1366.21	12.61	626.32	58.90	3058.57	243.91	2.23	132.66	0.12	BLD	BLD	16.07
	NMS-2-3	1.39	1786.34	2465.35	9.73	1061.00	47.07	1712.13	116.02	2.62	80.30	0.03	BLD	BLD	5.92
	NMS-2-4	5.11	2194.86	1510.91	12.80	753.26	65.98	2763.97	509.68	2.19	138.82	0.51	BLD	0.80	14.26
	NMS-2-5	69.77	11,629.06	1001.99	0.27	539.84	63.40	1166.09	483.56	1.57	107.47	7.56	0.09	1.57	BLD
	NMS-2-6	36.47	2351.52	1297.71	22.40	698.85	64.30	3385.32	272.11	1.92	133.64	1.40	0.45	2.81	16.37
	NMS-2-7	44.03	10,205.90	108.66	BLD	704.46	11.52	794.14	698.57	1.96	42.20	9.38	BLD	BLD	BLD
	NMS-2-8	78.66	15,171.51	600.38	BLD	713.76	39.94	333.94	767.74	1.97	17.86	11.75	BLD	BLD	BLD
	NMS-2-9	3.86	1525.91	2270.94	62.65	1035.60	36.13	1408.38	22.75	2.96	83.45	0.03	5.94	42.19	2.51
	NMS-2-10	49.94	1982.75	1093.54	40.61	563.08	39.31	3035.20	197.26	2.00	164.52	0.51	0.54	3.91	17.92
	Min.	1.39	1525.91	108.66	0.27	539.84	11.52	333.94	22.75	1.57	17.86	0.03	0.09	0.80	1.96
	Max.	78.66	15,171.51	5191.82	85.95	2024.89	65.98	3385.32	767.74	2.96	164.52	11.75	5.94	42.19	17.92
	Median	36.47	2258.26	1331.96	17.60	709.11	44.45	1560.25	258.01	2.10	95.46	0.51	0.54	3.36	14.26
	Average	32.58	5070.14	1690.75	30.88	872.11	46.84	1866.67	333.52	2.23	95.23	3.13	1.98	9.33	10.71
	S.D.	28.53	4899.40	1341.99	27.96	418.92	16.07	1041.99	254.10	0.42	45.62	4.33	2.21	14.75	6.46
NMS-5 $n = 9$	NMS-5-1	8.29	3980.66	2.78	0.45	BLD	1.19	4626.48	9.28	2.44	212.42	0.01	0.25	0.90	BLD
	NMS-5-2	34.27	1943.87	884.46	20.08	488.06	33.36	2554.53	193.72	2.26	142.49	1.19	0.07	0.85	10.78
	NMS-5-3	2.82	3322.38	4.32	0.31	2.40	0.78	5365.12	7.10	2.41	278.48	BLD	BLD	BLD	0.34
	NMS-5-4	44.14	5574.82	292.06	BLD	296.82	26.10	1321.07	542.55	1.72	42.49	2.15	BLD	BLD	BLD
	NMS-5-5	51.55	5677.35	383.21	BLD	312.78	29.80	1083.50	493.23	1.93	48.98	3.10	BLD	BLD	BLD
	NMS-5-6	2.85	1679.23	974.75	12.63	482.70	35.65	2106.33	224.25	2.48	121.12	0.04	0.02	BLD	13.60
	NMS-5-7	53.07	8194.90	47.47	BLD	27.47	2.34	3089.33	22.33	2.33	71.84	BLD	BLD	BLD	BLD
	NMS-5-8	5.71	1724.06	2669.10	49.38	1153.91	54.11	995.82	148.22	3.00	55.08	0.09	2.61	26.49	0.73
	NMS-5-9	9.42	1996.63	530.07	4.63	270.75	20.37	3029.74	140.93	2.54	175.38	0.17	0.08	1.09	11.64
	Min.	2.82	1679.23	2.78	0.31	2.40	0.78	995.82	7.10	1.72	42.49	0.01	0.02	0.85	0.34
	Max.	53.07	8194.90	2669.10	49.38	1153.91	54.11	5365.12	542.55	3.00	278.48	3.10	2.61	26.49	13.60
	Median	9.42	3322.38	383.21	8.63	304.80	26.10	2554.53	148.22	2.41	121.12	0.17	0.08	0.99	10.78
	Average	23.57	3788.21	643.14	14.58	379.36	22.63	2685.77	197.96	2.34	127.59	0.96	0.60	7.33	7.42
	S.D.	20.56	2153.90	792.28	17.06	337.53	17.30	1447.80	187.15	0.35	77.67	1.15	1.01	11.06	5.70
NMS-7 $n = 8$	NMS-7-1	3.89	2567.59	489.89	15.67	240.82	20.64	3601.98	158.27	2.65	189.52	0.02	BLD	BLD	13.52
	NMS-7-2	60.57	11,731.80	304.14	1.01	401.96	17.93	436.34	499.88	2.12	23.26	7.34	0.03	1.37	BLD
	NMS-7-3	144.33	15,271.94	940.19	0.52	540.53	63.74	424.42	682.66	1.93	87.63	15.05	0.06	2.67	0.34
	NMS-7-4	177.73	14,415.03	1018.49	2.45	567.10	69.51	445.94	656.87	1.94	126.48	21.78	0.47	6.28	0.22
	NMS-7-5	85.35	15,385.92	551.72	BLD	685.86	44.87	276.80	983.69	1.88	14.80	18.52	BLD	BLD	BLD
	NMS-7-6	2.90	3020.49	1322.35	50.91	555.34	16.23	3562.22	200.60	2.34	196.73	0.02	4.02	33.30	14.97
	NMS-7-7	7.75	3257.11	1062.29	2.65	576.17	52.68	3168.06	484.91	2.01	122.25	0.41	0.12	3.17	2.76
	NMS-7-8	10.80	3192.97	978.40	11.08	527.36	45.42	3509.59	424.68	1.87	147.07	0.52	0.41	7.89	4.35
	Min.	2.90	2567.59	304.14	0.52	240.82	16.23	276.80	158.27	1.87	14.80	0.02	0.03	1.37	0.22
	Max.	177.73	15,385.92	1322.35	50.91	685.86	69.51	3601.98	983.69	2.65	196.73	21.78	4.02	33.30	14.97
	Median	35.68	7494.46	959.29	2.65	547.93	45.14	1807.00	492.39	1.97	124.36	3.93	0.26	4.72	3.56
	Average	61.66	8605.36	833.43	12.04	511.89	41.38	1928.17	511.44	2.09	113.47	7.96	0.85	9.11	6.03
	S.D.	62.05	5739.59	304.98	15.74	130.38	19.93	1457.77	257.48	0.60	61.26	8.39	1.32	10.25	5.55

Table 1. *Cont.*

Sample ID	Spot No.	Mn	Fe	Cu	Ga	Ge	Ag	Cd	Pb	Co	Hg	Tl	In	Sn	Sb
NMS-10 $n = 7$	NMS-10-1	3.39	2803.48	1306.69	2.61	688.60	56.52	2932.11	371.69	1.98	145.62	1.70	BLD	BLD	13.84
	NMS-10-2	2.96	2821.35	1656.85	3.97	828.48	55.45	2942.67	411.12	2.09	146.42	0.08	BLD	BLD	14.26
	NMS-10-3	4.38	4790.85	7.90	3.18	1.19	1.29	6286.87	2.85	2.31	321.92	0.02	0.19	6.16	BLD
	NMS-10-4	3.13	2493.68	1232.51	19.92	631.79	44.39	2880.02	316.88	2.05	169.27	0.14	BLD	0.29	13.29
	NMS-10-5	1.36	2322.53	1563.03	21.13	746.85	21.77	2521.65	301.71	2.29	131.45	0.04	BLD	BLD	11.74
	NMS-10-6	1.29	2351.22	1136.79	6.98	584.54	35.70	2632.58	326.53	2.07	125.92	0.02	BLD	BLD	9.29
	NMS-10-7	70.77	2871.43	1514.86	1.93	772.40	63.10	3276.86	317.01	1.91	141.28	2.47	BLD	1.54	7.53
	Min.	1.29	2322.53	7.90	1.93	1.19	1.29	2521.65	2.85	1.91	125.92	0.02	0.19	0.29	7.53
	Max.	70.77	4790.85	1656.85	21.13	828.48	63.10	6286.87	411.12	2.31	321.92	2.47	0.19	6.16	14.26
	Median	3.13	2803.48	1306.69	3.97	688.60	44.39	2932.11	317.01	2.07	145.62	0.08	0.19	1.54	12.51
	Average	12.47	2922.08	1202.66	8.53	607.69	39.75	3353.25	292.54	2.10	168.84	0.64	0.19	2.66	11.66
	S.D.	23.82	791.74	517.84	7.74	259.33	20.40	1218.48	123.45	0.14	63.78	0.94	0.00	2.53	2.48
NMS-14 $n = 8$	NMS-14-1	65.56	14,588.81	179.84	BLD	631.20	15.99	531.72	1235.21	1.90	46.64	9.14	BLD	BLD	BLD
	NMS-14-2	2.71	2828.70	1016.89	22.30	466.81	37.14	3759.95	259.70	2.11	187.21	0.05	0.36	7.69	19.63
	NMS-14-3	15.97	2246.54	1885.02	27.66	802.82	47.10	2584.62	208.92	2.24	155.08	0.37	0.09	0.20	12.55
	NMS-14-4	21.83	4628.39	1071.64	BLD	642.09	238.37	1992.45	873.42	1.41	72.42	0.69	BLD	BLD	BLD
	NMS-14-5	41.35	9110.29	530.27	18.22	447.72	49.44	1096.14	591.05	1.66	96.59	6.01	0.25	0.81	BLD
	NMS-14-6	43.24	10,450.27	89.05	BLD	524.40	10.28	947.50	677.07	1.66	67.70	7.55	BLD	BLD	BLD
	NMS-14-7	49.08	3327.04	681.20	6.47	408.88	53.33	3812.57	237.45	1.63	180.04	8.80	0.33	2.57	19.70
	NMS-14-8	85.86	14,429.99	1021.45	9.05	783.46	123.61	347.06	990.70	1.67	55.62	24.73	0.16	1.84	BLD
	Min.	2.71	2246.54	89.05	6.47	408.88	10.28	347.06	208.92	1.41	46.64	0.05	0.09	0.20	12.55
	Max.	85.86	14,588.81	1885.02	27.66	802.82	238.37	3812.57	1235.21	2.24	187.21	24.73	0.36	7.69	19.70
	Median	42.30	6869.34	849.04	18.22	577.80	48.27	1544.30	634.06	1.67	84.51	6.78	0.25	1.84	19.63
	Average	40.70	7701.25	809.42	16.74	588.42	71.91	1884.00	634.19	1.78	107.66	7.17	0.24	2.62	17.29
	S.D.	25.36	4800.11	538.91	7.96	141.26	70.69	1295.65	358.43	0.26	53.86	7.54	0.10	2.66	3.35

BLD means concentration below the detection limit.

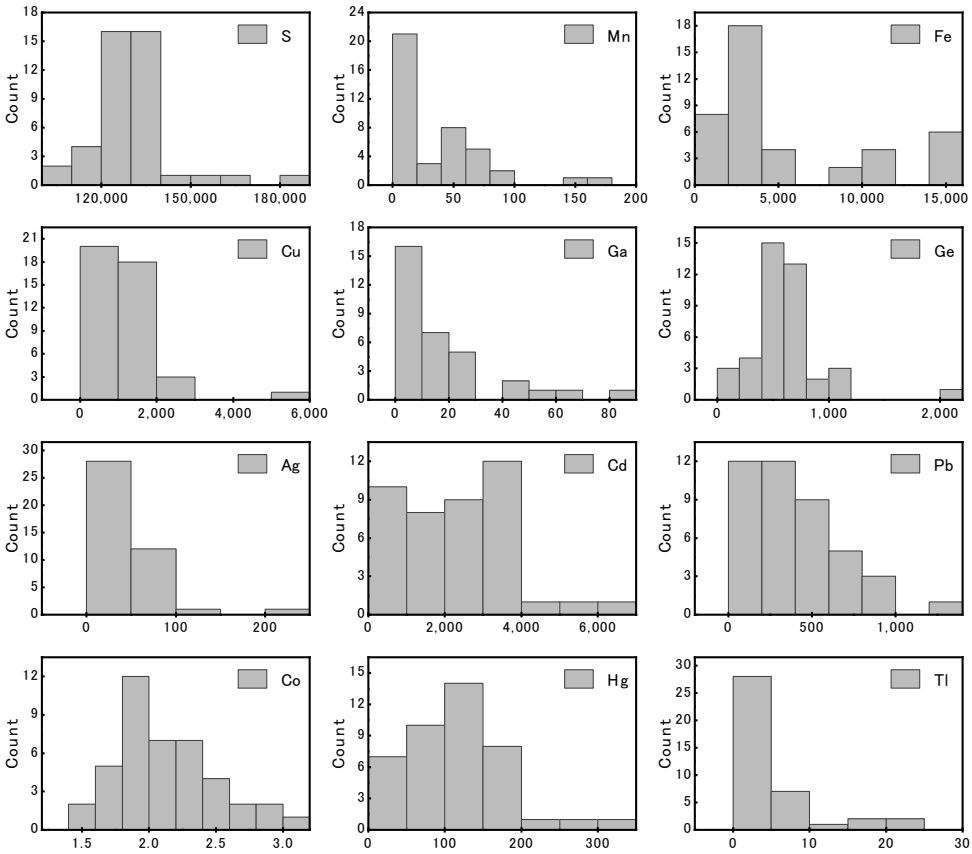

Figure 5. *Cont.*

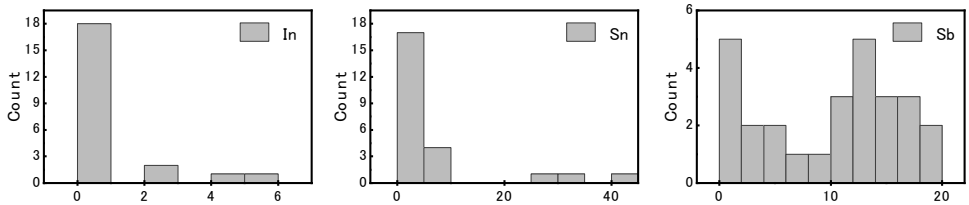

Figure 5. Histogram of trace element composition of sphalerite in Nanmushu deposit.

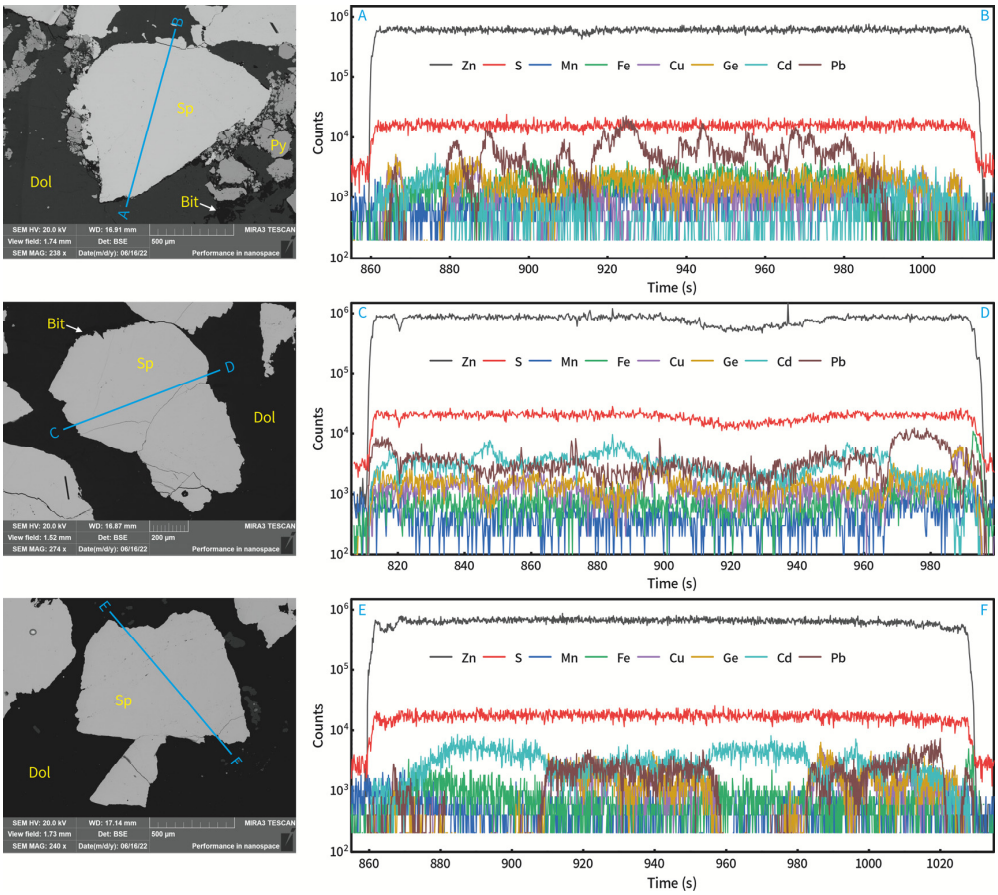

Figure 6. A backscattered electron image of sphalerite and its LA-ICP-MS linear scan profiles. Abbreviations are the same as in Figure 4.

Among these trace elements, Fe concentration was the highest, ranging from 1525.91 ppm to 15,385.92 ppm, with an average of 5741.24 ppm. The following trace elements were Cd and Cu, whose contents varied from 276.80 ppm to 6286.87 ppm (with an average of 2349.37 ppm) and from 2.78 ppm to 5191.82 ppm (with an average of 1123.90 ppm), respectively. Sphalerite also contains abundant trace elements Ge, Pb, and Hg. Their concentrations varied from 1.19 ppm to 2024.89 ppm (with an average of 624.15 ppm), 2.85 ppm to 1235.21 ppm (with an average of 399.27 ppm), and 14.80 ppm to 321.92 ppm (with an average of 122.46 ppm), respectively. The average content of Ag, Mn, Ga, and Sb is less than 50 ppm, whose average contents are 44.20 ppm, 34.43 ppm, 17.04 ppm, and 10.00 ppm, respectively. Besides, sphalerite contains minor trace elements Sn, Tl, Co, and In, the average content of which is less than 10 ppm. Sphalerite from the Nanmushu deposit contains high concentrations of Ag, Ge, Cd, and Cu elements, which exceed the minimum grades required for their extraction and utilization in China. These grades are 2 ppm for Ag, 10 ppm for Ge, 100 ppm for Cd, and 600 ppm for Cu. Therefore, these elements may be recovered through mineral processing or smelting techniques.

5. Discussion

5.1. Occurrence of Trace Elements in Sphalerite

This paper examines the occurrence states of trace elements in sphalerite by using three methods: contents histogram, LA-ICP-MS time-resolved depth profiles, and linear scan profiles [38,39]. The contents histogram shows that Cu, Ge and Pb have a wide range of concentrations in sphalerite, from 2.78 ppm to 5191.82 ppm, from 1.19 ppm to 2024.89 ppm, and from 2.85 ppm to 1235.21 ppm, respectively (Table 1). The LA-ICP-MS linear scan reveals that Pb has a large variation in the three curves (Figure 6). The time-resolved depth profiles indicate that most test spots have flat curves with small fluctuations in trace elements (Figure 7a), while some test spots have large fluctuations in Pb (Figure 7b,e) and Ag (Figure 7e), moderate fluctuations in Fe (Figure 7d), and smooth fluctuations in Ge, Cu, and Mn (Figure 7c,f).

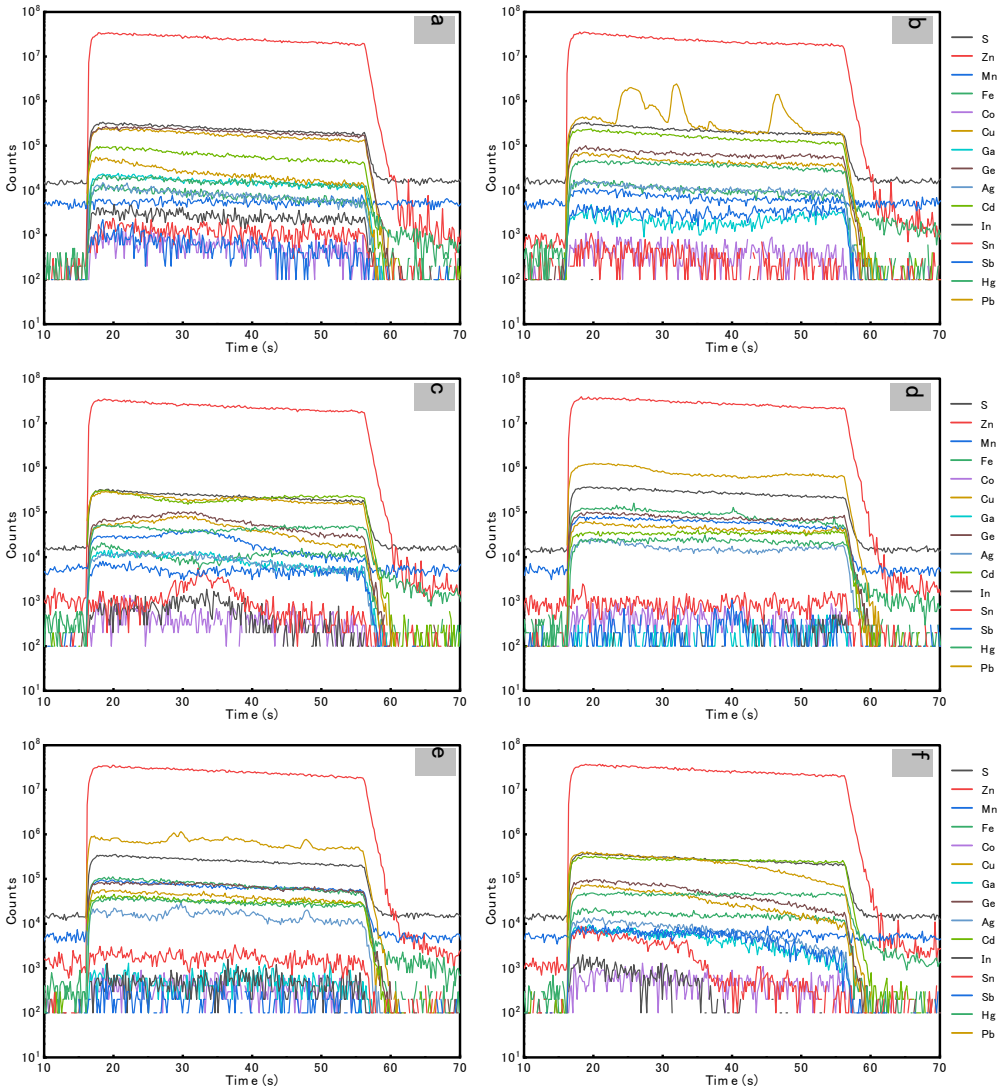

Figure 7. Representative time-resolved depth profiles for selected elements in sphalerite analyzed in this study. (**a**) The stable test signals indicate that trace elements occur as isomorphism in sphalerite; (**b**) The signal curves of Pb show large fluctuation; (**c**) The signal curves of Ge, Cu, and Mn show smooth fluctuation; (**d**) The signal curve of Fe shows moderate fluctuation; (**e**) The signal curves of Pb and Ag show large fluctuation; (**f**) The signal curves of Ge, Cu, and Pb show smooth fluctuation.

The results suggest that Pb, Fe, and Ag have different occurrence states in sphalerite besides isomorphism. The micrograph and BSE electron photograph show that some

minerals such as pyrite are included in sphalerite (Figures 4d and 6). The time-resolved depth profiles and linear scan profiles show that Pb, Fe, and Ag have large fluctuations in some test spots (Figure 7b,e), indicating the presence of inclusions. The other trace elements have small variations in their concentration and smooth curves, indicating that they mainly occur as isomorphism in sphalerite particles.

5.2. Substitution Mechanisms of Zn by Trace Elements

5.2.1. Iron Element

Fe is the most enriched trace element in sphalerite from the Nanmushu deposit. The correlation between Fe and other trace elements can reveal whether Fe facilitates the substitution of Zn by other trace elements in sphalerite. The scatter plot shows that Fe has a positive correlation with Mn, Pb, and Tl, with correlation coefficients (R^2) of 0.66, 0.58, and 0.79, respectively (Figure 8a–c). Previous studies have suggested that divalent cations, such as Fe^{2+}, Mn^{2+}, and Cd^{2+}, can directly replace Zn^{2+} in sphalerite because they have similar ion radii and oxidation states in tetrahedral coordination [3,5,40,41]. Pb^{2+} can also enter the sphalerite structure by simple substitution for Zn^{2+} [38,42], while monovalent (Ag^{+} and Cu^{+}) or trivalent (In^{3+}, Ga^{3+}, Fe^{3+}, and Tl^{3+}) cations can enter the sphalerite structure by coupled substitution for Zn^{2+} [43]. Therefore, Fe^{2+} in sphalerite can easily form isomorphism with Mn^{2+}, Pb^{2+}, and Tl^{3+} by substituting Zn^{2+}.

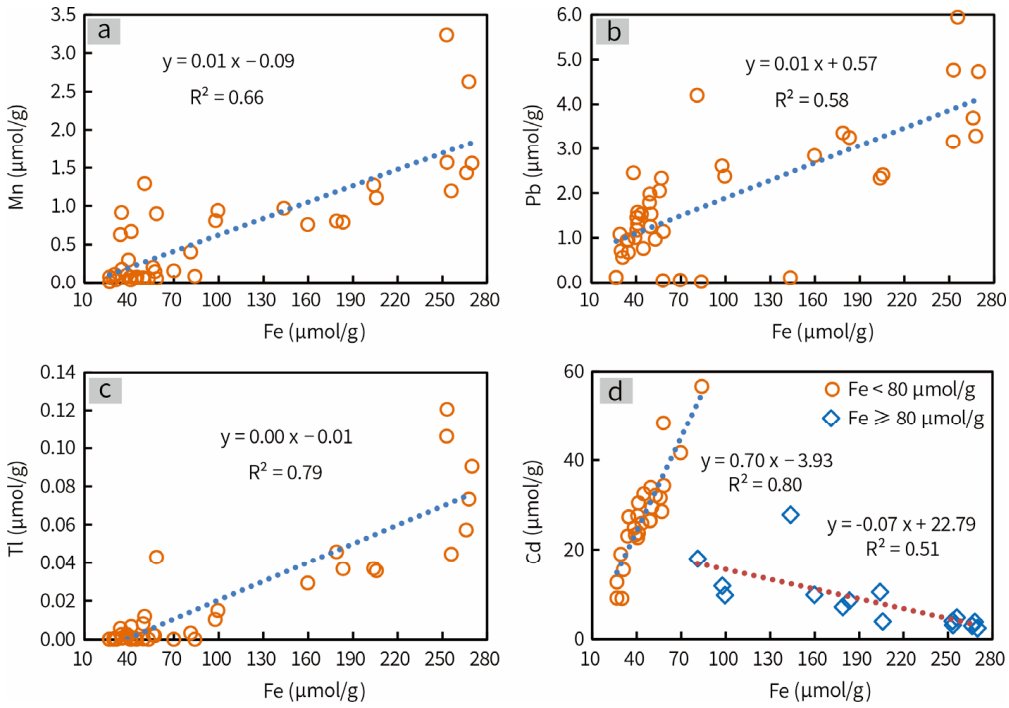

Figure 8. Plots of (**a**) Fe vs. Mn; (**b**) Fe vs. Pb; (**c**) Fe vs. Tl; (**d**) Fe vs. Cd.

The scatter plot also shows that Cd has a different relationship with Fe than other trace elements. Cd has a positive correlation with Fe at lower concentrations (R^2 = 0.82), but it has a negative correlation with Fe at higher concentrations (R^2 = 0.51) (Figure 8d). This suggests that low concentration Fe occurs as an isomorph in sphalerite and co-substitutes Zn^{2+} with Cd^{2+}, while high concentration Fe may be mainly due to Fe mineral inclusions (Figure 4d), which have low Cd content but high Mn, Pb, and Tl content (Figure 8a–c). Therefore, the occurrence state of Fe in sphalerite affects the substitution of Cd for Zn.

5.2.2. Cadmium Element

Sphalerite is the main carrier of the dispersed element Cd [4,44]. The scatter plot shows that Cd has a good positive correlation with Hg (R^2 = 0.83) (Figure 9a), but it

has a negative correlation with Pb, Mn, and Tl (R^2 = 0.44, 0.35, and 0.39, respectively) (Figure 9b–d). In contrast, Pb and Mn, Pb and Tl, and Mn and Tl have positive correlations with each other (R^2 = 0.32, 0.51, and 0.74, respectively) (Figure 9e–g). Overall, (Cd + Hg) and (Mn + Pb + Tl) have a good negative correlation (R^2 = 0.49) (Figure 9h). This implies that the trace elements Cd and Hg coexist in sphalerite, or Mn, Pb, and Tl co-substitute Zn in sphalerite; that is, $(2Mn, 2Pb, 3Tl)^{6+}$, $3(Cd, Hg)^{2+}) \leftrightarrow 3Zn^{2+}$.

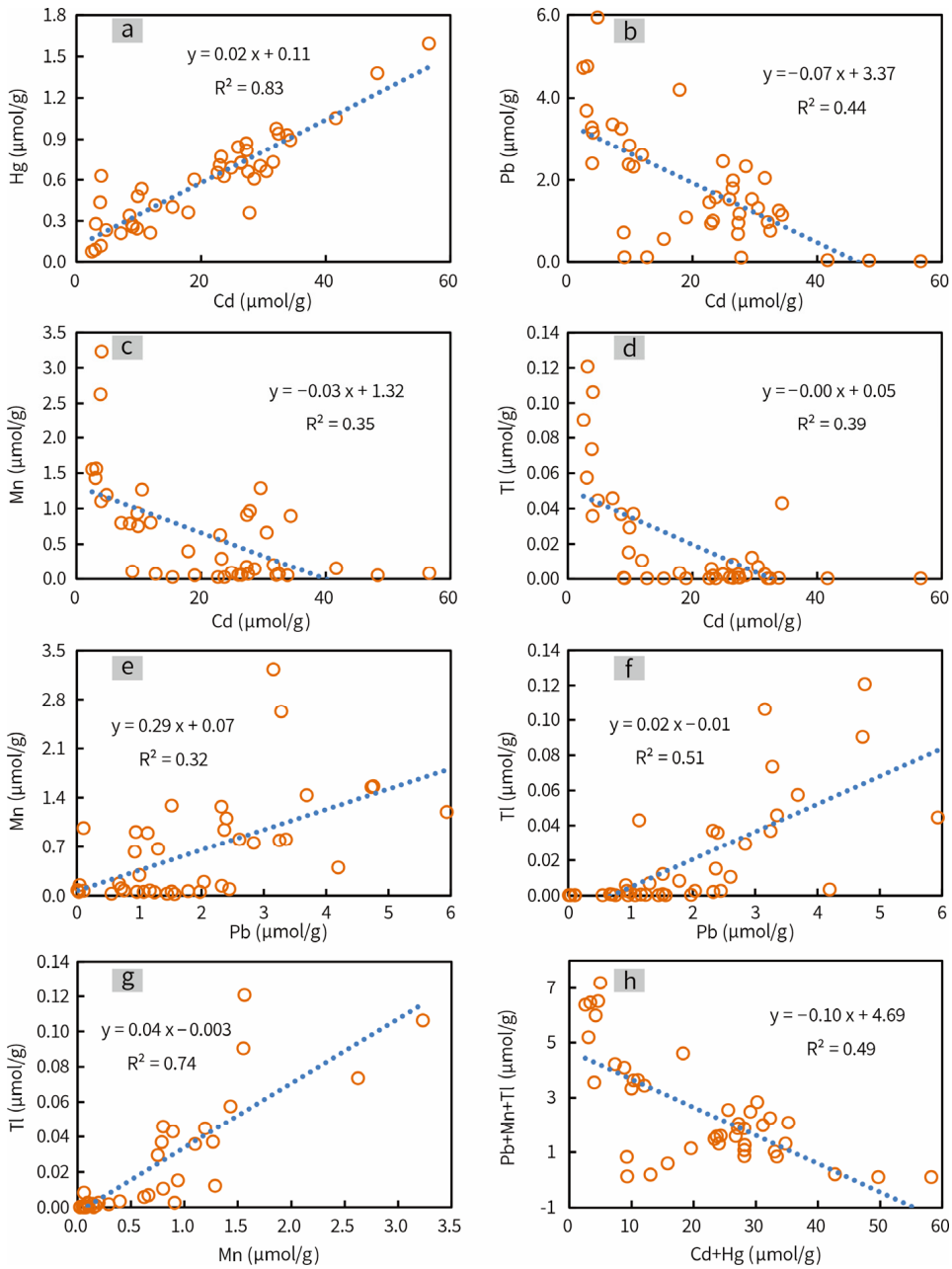

Figure 9. Plots of (**a**) Cd vs. Hg; (**b**) Cd vs. Pb; (**c**) Cd vs. Mn; (**d**) Cd vs. Tl; (**e**) Pb vs. Mn; (**f**) Pb vs. Tl; (**g**) Mn vs. Tl; (**h**) (Cd + Hg) vs. (Pb + Mn + Tl).

5.2.3. Germanium Element

The present study shows that germanium occurs in sphalerite mainly in two forms: independent minerals (mineral inclusions) and isomorphism. Ge minerals are rarely found in sphalerite, and most Ge occurs as isomorphs. However, the substitution mechanism of Ge varies depending on the deposits. Even within the same deposit, Ge may have multiple ways of replacing Zn. For example, Ge can directly replace Zn in sphalerite:

$Ge^{4+} \leftrightarrow 2Zn^{2+}$ or $Ge^{2+} \leftrightarrow Zn^{2+}$ [5,45,46]. In the Saint-Salvy deposit in France, Ge has two other substitution methods: $2Cu^{+} + Cu^{2+} + Ge^{4+} \leftrightarrow 4Zn^{2+}$ [47] and $2Ag^{+}/Cu^{+} + Ge^{4+} \leftrightarrow 3Zn^{2+}$ [40]. In the lead–zinc deposits around the Yangtze Block in China, Ge has more diverse substitution methods, such as $2Cu^{+} + Ge^{4+} \leftrightarrow 3Zn^{2+}$ [31,48,49], $2Fe^{2+} + Ge^{4+} + \square \leftrightarrow 4Zn^{2+}$ ($\square$ represents vacancy) [50], $nCu^{2+} + Ge^{2+} \leftrightarrow (n + 1)\ Zn^{2+}$ [51], $Fe + Ge \leftrightarrow 2Zn$ [52], and $Mn^{2+} + Ge^{2+} \leftrightarrow 2(Zn, Cd)^{2+}$ [53] etc.

The scatter plot shows that Ge has a good correlation with Cu in the sphalerite of the Nanmushu deposit ($R^2 = 0.82$) (Figure 10a). Ge and Ga and Ga and Cu also have positive correlations with each other, with R^2 values of 0.47 and 0.56, respectively (Figure 10b,c). Overall, (Ge + Ga) and Cu have a better positive correlation, with R^2 reaching 0.84 (Figure 10d). In minerals, Ge usually has 2 oxidation states of +4 and +2, and Cu usually has 2 oxidation states of +2 and +1. μ-XANES studies indicate that Ge and Cu mainly exist as Ge^{4+} and Cu^{+} in sphalerite, rather than +2 valence [54–56]. It has been shown that Ga often replaces Zn^{2+} with +3 valence in sphalerite [5,41,57,58]. Therefore, a possible substitution mechanism of Ge and Ga in the Nanmu deposit is $Ge^{4+} + 2Cu^{+} \leftrightarrow 3Zn^{2+}$ or $2Ga^{3+} + 2Cu^{+} \leftrightarrow 4Zn^{2+}$.

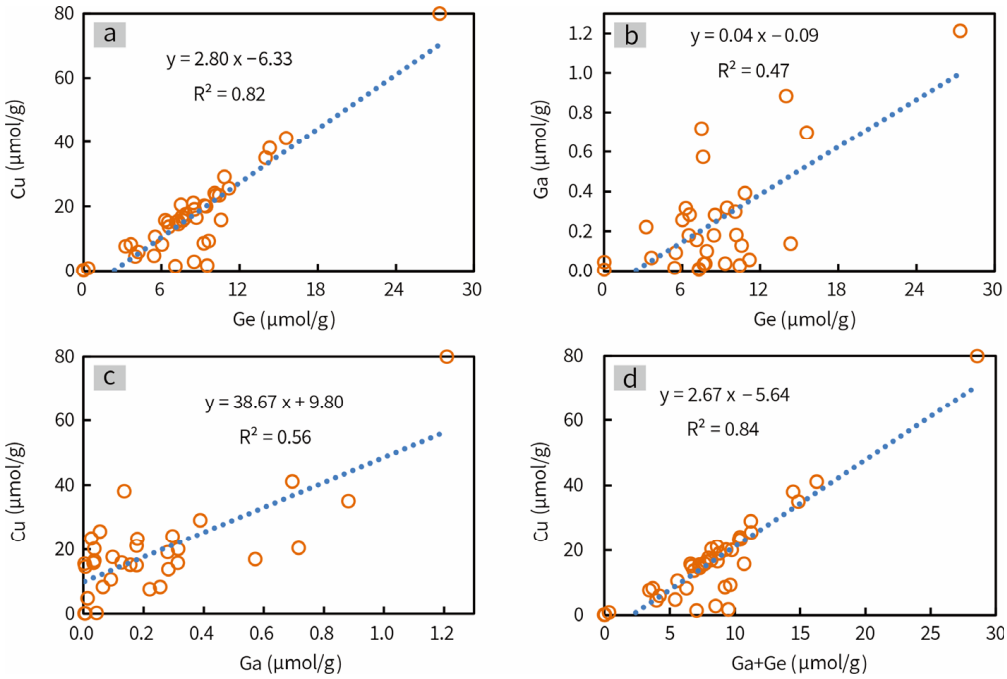

Figure 10. Plots of (**a**) Ge vs. Cu; (**b**) Ge vs. Ga; (**c**) Ga vs. Cu; (**d**) (Ga + Ge) vs. Cu.

5.3. Ore-Forming Temperature

Previous studies have suggested that the trace elements in sphalerite are related to the ore-forming temperature. Since Fe^{2+}, Mn^{2+}, In^{3+}, and Zn^{2+} have very similar ionic radii, and Se, Te, and S have similar geochemical characteristics, they can easily substitute each other in sphalerite under relatively high temperature conditions [3,59]. Dark sphalerite with high concentrations of Fe, Mn, In, Se, and Te is usually formed at higher temperatures with higher In/Ga ratios, while light sphalerite with high concentrations of Cd, Ga, and Ge is often formed at lower temperatures with lower In/Ge ratios [50,60]. The sphalerite in the Nanmushu deposit is dominated by tawny or brown and is characterized by Cd and Ge enrichment with low In/Ge ratios (<0.16), suggesting a lower formation temperature.

Frenzel et al. (2016) established a relationship between the trace element compositions of sphalerite and homogenization temperatures and concluded that Mn, Fe, and In increase while Ga and Ge decrease in sphalerite with increasing temperatures of deposition [1]. A strong correlation between PC 1* and the homogenization temperature, as suggested by Frenzel et al. (2016), shows that this expression can be used as a geothermometer (GGIMFis)

and is widely applied in the study of ore-forming temperatures [61–63]. The empirical relationship between PC 1* and the homogenization temperature is as follows:

$$T\ (^{\circ}C) = -(54.4 \pm 7.3) \times PC\ 1^{*} + (208 \pm 10)$$

The expression of PC 1* is:

$$PC\ 1^{*} = \ln\left[\left(C_{Ga}^{0.22} \times C_{Ge}^{0.22}\right) / \left(C_{Fe}^{0.37} \times C_{Mn}^{0.20} \times C_{In}^{0.11}\right)\right]$$

with Ga, Ge, In, and Mn concentrations in ppm, while Fe concentration is in wt%.

From this study, the ore-forming temperature of the Nanmushu deposit calculated by the GGIMFis geothermometer ranges from 24 to 199 °C, with an average of 116 °C. As the samples in this study are not extensive, the calculated temperature range is lower than that of previous homogenization temperatures of fluid inclusions in sphalerite, quartz, dolomite, barite, and calcite from the Nanmushu deposit (107–340 °C) [19]. Based on the two geothermometer criteria discussed above, it can be inferred that the Nanmushu deposit originated from a medium-low temperature environment.

5.4. Genesis of Ore Deposit

The trace elements in sphalerite can reflect the genetic type of ore deposits because they are influenced by the physical and chemical conditions of mineralization, the sources of ore-forming materials, the fluid migration and precipitation mechanism, and the types of minerals [3,5,64]. Generally, epithermal deposits have high concentrations of Fe, Cu, Ga, In, Mn, and Sn and low concentrations of Ge and Pb; MVT Pb–Zn deposits have high concentrations of Ag, Ge, and Sb and low concentrations of Co, Cu, Fe, In, and Mn; SEDEX Pb–Zn deposits have high concentrations of Ag, Fe, Pb, and Sb and low concentrations of Cd, Co, Ga, Ge, and Mn; Skarn Pb–Zn deposits have high concentrations of Fe, Mn, Co, and In and low concentrations of Ga, Sb, and Ag; and VMS Pb–Zn deposits have high concentrations of Cd, Fe, Ga, and Mn and low concentrations of Cu, Ge, Pb, Ag, and Sn (Figure 11). The Nanmushu deposit has a trace element composition similar to that of MVT Pb–Zn deposits.

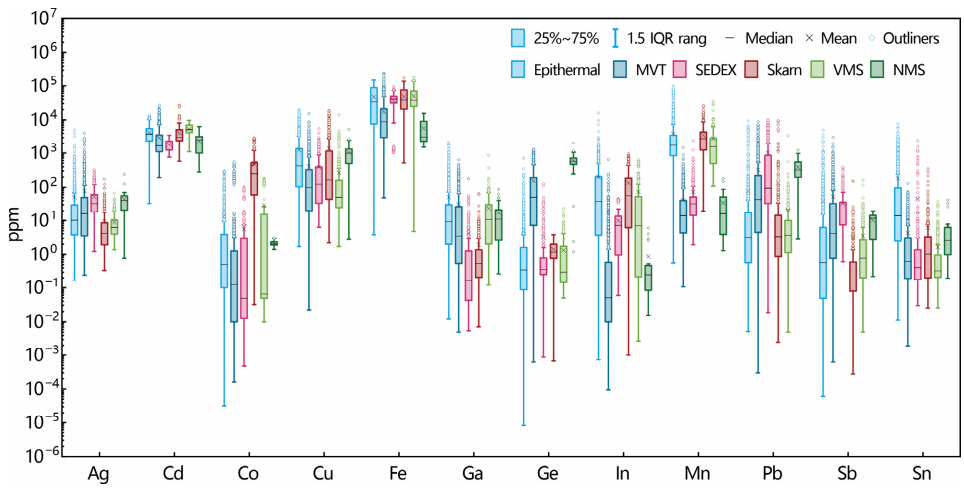

Figure 11. Box plots of trace elements in sphalerite from the Nanmushu deposit and five Pb–Zn deposit types. Epithermal data are collected from references [5,13,14,65–71]; MVT data are collected from references [3,5,18,30,41–43,50,66,72–74]; SEDEX data are collected from references [75–79]; Skarn data are collected from references [3,5,13,14,67,80–82]; and VMS data are collected from references [3,5,66,83,84].

In the lnGa–lnIn diagram of sphalerite trace elements [85,86], the samples from the Nanmushu deposit mostly fall into the field of sedimentary-reworked deposit (Figure 12).

Moreover, the ternary plots of Ag–(Ga + Ge)–(In + Se + Te) (Figure 13a) and Cd–Mn–1000 Ge (Figure 13b) of sphalerite are often used to determine the genesis of lead–zinc deposits [87–89]. In these ternary plots, the Nanmushu sphalerite also falls into the MVT field, which is clearly different from the SEDEX, VMS, and Skarn deposits.

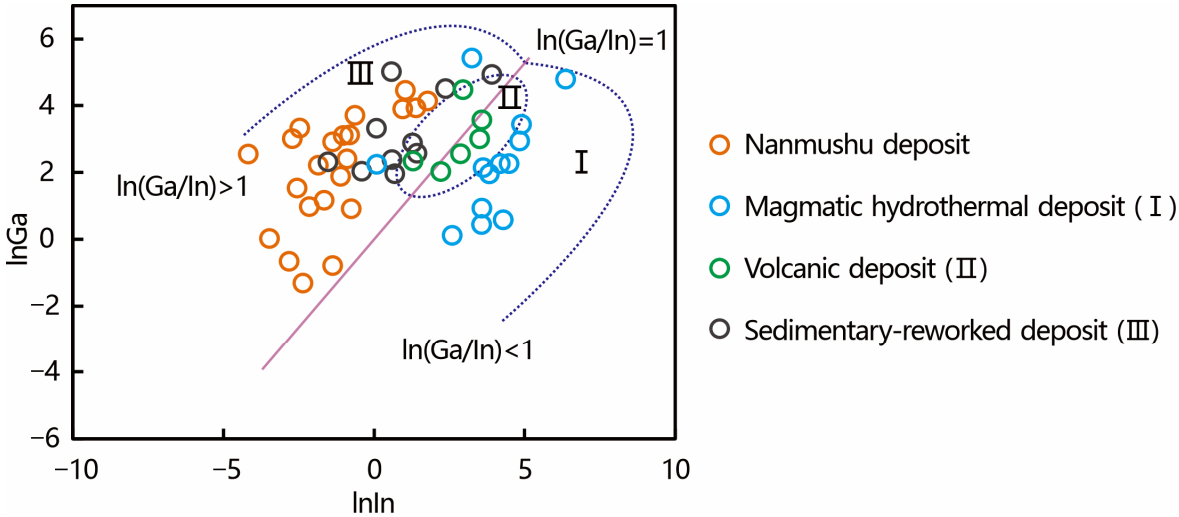

Figure 12. Plot of ln(Ga) vs. ln(In) for sphalerite from different Pb–Zn deposit types (modified after reference [85,86]).

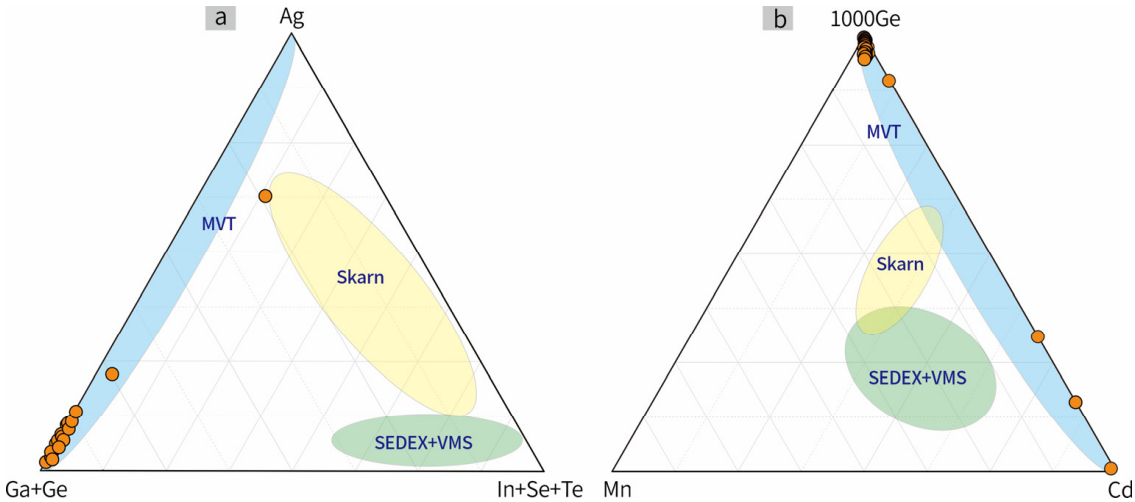

Figure 13. Ternary Ag–(Ga + Ge)–(In + Se + Te) plot (**a**) and Cd–Mn–1000Ge plot (**b**) of sphalerite from the Daliang deposit (modified after reference [87–89]).

In the Ge–In and Ge–Mn relation diagrams of sphalerite trace elements, most samples from the Nanmushu deposit plot into the range of the MVT deposit. However some test points deviate from the MVT field (Figure 14a,b) which is related to the Ge enrichment of sphalerite in the Nanmushu deposit. In the Cd/Fe–Mn and Mn–Fe diagrams, the test points from the Nanmushu deposit almost all plot into the range of the MVT deposit (Figure 14c,d).

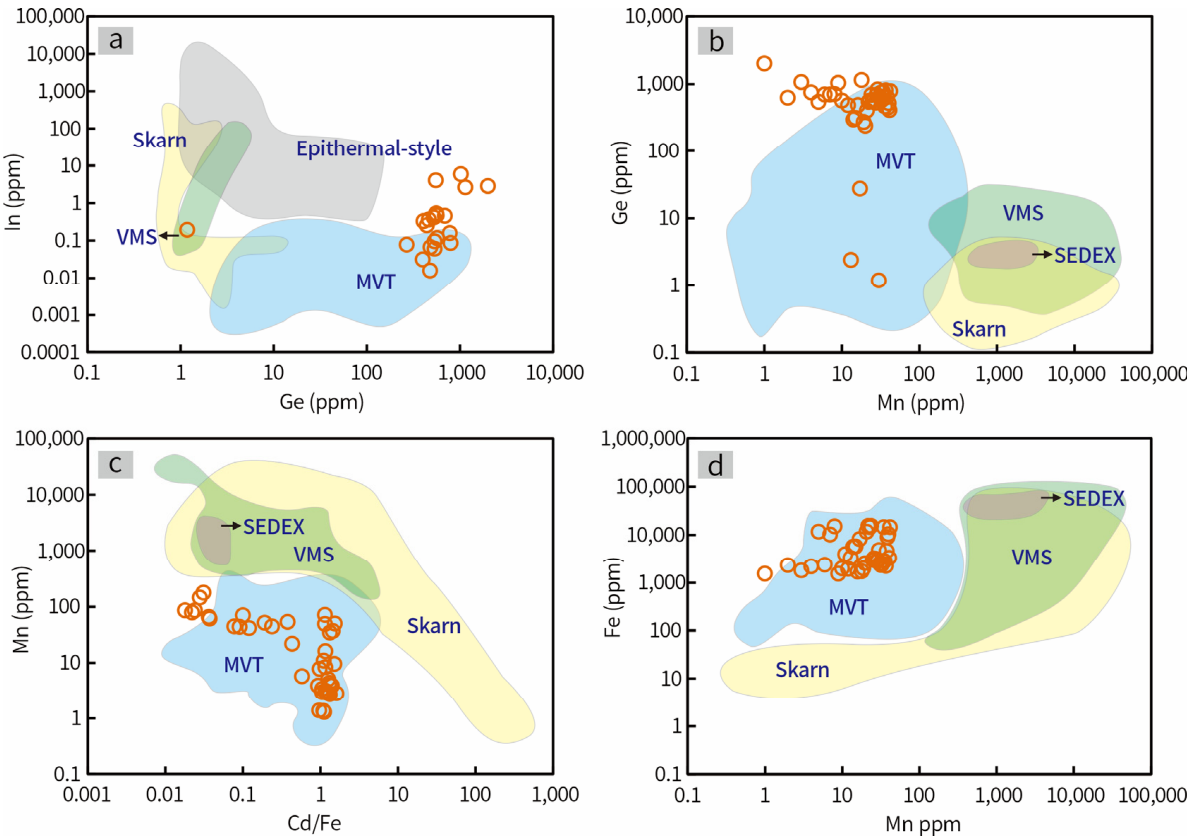

Figure 14. Plots of Ge vs. In. (**a**): Mn vs. Ge; (**b**) Cd/Fe vs. Mn; (**c**) Mn vs. Fe (**d**); (modified after reference [41]).

The ore bodies from the Nanmushu deposit are stratiform or stratiform-like along the brecciform dolostone of the Sinian Dengying Formation. They are related to the paleo oil reservoir but not associated with igneous activity [21,25,26]. Previous studies show that the ore-forming ages are mainly 468–488 Ma [21–23], suggesting that Nanmu belongs to an epigenetic hydrothermal deposit. Furthermore, the ore-forming fluids are basinal brines trapped in a heterogenous fluid system with medium-low temperature and medium-high salinity [19]. Sulfur and lead isotopes indicate that ore-forming sulfur originated from the thermochemical sulfate reduction (TSR) of seawater or evaporitic sourced sulfates and a mixing of lead from the basement and the host rocks [16]. The Cambrian Guojiaba Formation may have provided not only the oil for the paleo oil reservoir but also the ore metals for the Pb–Zn mineralization [25]. As reducing agents of TSR, reaction hydrocarbon organic matter plays an important role in mineralization [21,26]. This study and previous data revealed that the features of Nanmushu are consistent with those of MVT Pb–Zn deposit [90,91]. Therefore, we concluded that Nanmushu belongs to an MVT deposit.

6. Conclusions

(1) Sphalerite from the Nanmushu deposit contains various trace elements, such as Mn, Fe, Cu, Ga, Ge, Ag, Cd, Pb, Co, Hg, Tl, In, Sn, and Sb. Among them, Ag, Ge, Cd, and Cu are valuable components that may be recovered during mineral processing or smelting techniques.

(2) Most of the trace elements in sphalerite occur as isomorphs, while a small amount of Pb, Fe, and Ag occur as tiny mineral inclusions. Zn^{2+} can be easily substituted by Fe^{2+}, Mn^{2+}, Pb^{2+}, and Tl^{3+} in the form of isomorphism, Cd^{2+} and Hg^{2+} together, or Mn^{2+}, Pb^{2+}, and Tl^{3+} together to replace Zn^{2+}; that is, $(3Mn, 3Pb, 2Tl)^{6+}$, $3(Cd, Hg)^{2+}$) $\leftrightarrow 3Zn^{2+}$. Cu^{+} exhibits a tendency to combine with Ge^{4+} or Ga^{3+} to substitute for Zn^{2+}; that is, $Ge^{4+} + 2Cu^{+} \leftrightarrow 3Zn^{2+}$ or $2Ga^{3+} + 2Cu^{+} \leftrightarrow 4Zn^{2+}$.

(3) Trace element compositions of the Nanmushu sphalerite indicate that Zn mineralization occurred under low-temperature conditions (<200 °C). Based on previous studies, we comprehensively believe that Nanmushu is an MVT deposit.

Author Contributions: Conceptualization, H.D., Y.C. and S.X.; investigation, J.W., Y.C., S.X. and Q.N.; data curation, J.W.; writing—original draft preparation, J.W.; writing—review and editing, H.D., Y.C., S.X., Y.W. and P.L.; supervision, H.D. and Y.C.; funding acquisition, H.D. and Y.C. All authors have read and agreed to the published version of the manuscript.

Funding: This research was funded by the National Natural Science Foundation of China [grant number 51764023], the Research Fund of the Yunnan Provincial Department of Education [grant number 2022J1304], and the Kunming University of Science and Technology 2020 Top Innovative Talents Program for postgraduates- [grant number CA22369M111A].

Data Availability Statement: The data presented in this study are available on reasonable request from the corresponding authors.

Acknowledgments: We would like to express special thanks to Jiaxi Zhou for the invitation. The authors thank the three anonymous reviewers for their valuable comments and suggestions for improving the manuscript.

Conflicts of Interest: The authors declare no conflict of interest.

References

1. Frenzel, M.; Hirsch, T.; Gutzmer, J. Gallium, germanium, indium, and other trace and minor elements in sphalerite as a function of deposit type—A meta-analysis. *Ore Geol. Rev.* **2016**, *76*, 52–78. [CrossRef]
2. Luo, K.; Cugerone, A.; Zhou, M.; Zhou, J.; Sun, G.; Xu, J.; He, K.; Lu, M. Germanium enrichment in sphalerite with acicular and euhedral textures: An example from the Zhulingou carbonate-hosted Zn(-Ge) deposit, South China. *Miner. Deposita* **2022**, *57*, 1343–1365. [CrossRef]
3. Ye, L.; Cook, N.J.; Ciobanu, C.L.; Liu, Y.; Zhang, Q.; Liu, T.; Gao, W.; Yang, Y.; Danyushevskiy, L. Trace and minor elements in sphalerite from base metal deposits in South China: A LA-ICPMS study. *Ore Geol. Rev.* **2011**, *39*, 188–217. [CrossRef]
4. Liu, Y.C.; Hou, Z.Q.; Yue, L.L.; Ma, W.; Tang, B.L. Critical metals in sediment-hosted Pb-Zn deposits in China. *Chin. Sci. Bull.* **2022**, *67*, 406–424. [CrossRef]
5. Cook, N.J.; Ciobanu, C.L.; Pring, A.; Skinner, W.; Shimizu, M.; Danyushevsky, L.; Saini-eidukat, B.; Melcher, F. Trace and minor elements in sphalerite: A LA-ICPMS study. *Geochim. Cosmochim. Acta* **2009**, *73*, 4761–4791. [CrossRef]
6. Sun, G.; Zhou, J. Application of Machine Learning Algorithms to Classification of Pb–Zn Deposit Types Using LA–ICP–MS Data of Sphalerite. *Minerals* **2022**, *12*, 1293. [CrossRef]
7. Sahlström, F.; Arribas, A.; Dirks, P.; Corral, I.; Chang, Z. Mineralogical Distribution of Germanium, Gallium and Indium at the Mt Carlton High-Sulfidation Epithermal Deposit, NE Australia, and Comparison with Similar Deposits Worldwide. *Minerals* **2017**, *7*, 213. [CrossRef]
8. Jaskula, B. Gallium. In *US Geological Survey Mineral Commodity Summaries*; US Geological Survey: Reston, VA, USA, 2017; pp. 64–65. Available online: https://minerals.usgs.gov/minerals/pubs/commodity/gallium/mcs-2017-galli.pdf (accessed on 15 September 2017).
9. Guberman, D. Germanium. In *US Geological Survey Mineral Commodity Summaries*; US Geological Survey: Reston, VA, USA, 2017; pp. 70–71. Available online: https://minerals.usgs.gov/minerals/pubs/commodity/germanium/mcs-2017-germa.pdf (accessed on 15 September 2017).
10. Li, X.F.; Zhu, Y.T.; Xu, J. Indium as a critical mineral: A research progress report. *Chin. Sci. Bull.* **2020**, *65*, 3678–3687. [CrossRef]
11. Werner, T.; Mudd, G.M.; Jowitt, S.M. The world's by-product and critical metal resources part III: A global assessment of indium. *Ore Geol. Rev.* **2017**, *86*, 939–956. [CrossRef]
12. Hayes, S.M.; Mccullough, E.A. Critical minerals: A review of elemental trends in comprehensive criticality studies. *Resour. Policy* **2018**, *59*, 192–199. [CrossRef]
13. Zhang, J.; Shao, Y.; Liu, Z.; Chen, K. Sphalerite as a record of metallogenic information using multivariate statistical analysis: Constraints from trace element geochemistry. *J. Geochem. Explor.* **2022**, *232*, 106883. [CrossRef]
14. Xing, B.; Mao, J.; Xiao, X.; Liu, H.; Zhang, C.; Guo, S.; Li, H.; Huang, W.; Lai, C. Metallogenic discrimination by sphalerite trace element geochemistry: An example from the Fengyan Zn-Pb deposit in central Fujian, SE China. *Ore Geol. Rev.* **2022**, *141*, 104651. [CrossRef]
15. Hou, M.T.; Wang, D.G.; Deng, S.B.; Yang, Z.R. Geology and genesis of the Mayuan lead-zinc mineralization belt in the Shaanxi Province. *Northwest. Geol* **2007**, *40*, 42–60. (In Chinese with English Abstract)

16. Xiong, S.; Jiang, S.; Ma, Y.; Liu, T.; Zhao, K.; Jiang, M.; Zhao, H. Ore genesis of Kongxigou and Nanmushu Zn-Pb deposits hosted in Neoproterozoic carbonates, Yangtze Block, SW China: Constraints from sulfide chemistry, fluid inclusions, and in situ S-Pb isotope analyses. *Precambrian Res.* **2019**, *333*, 105405. [CrossRef]
17. Wang, X.H.; Xue, C.J.; Li, Z.M.; Li, Q.; Yang, R.J. Geological and geochemical characteristics of Mayuan Pb-Zn ore deposit on northern margin of Yangtze landmass. *Miner. Depos.* **2008**, *27*, 37–48. (In Chinese with English Abstract)
18. Gao, Y.B.; Li, K.; Qian, B.; Li, W.Y.; Zheng, M.C.; Zhang, C.G. Trace elements, S, Pb, He, Ar and C isotopes of sphalerite in the Mayuan Pb-Zn deposit, at the northern margin of the Yangtze Plate, China. *Acta Petrol. Sin.* **2016**, *32*, 251–263. (In Chinese with English Abstract)
19. Xiong, S.-F.; Gong, Y.-J.; Yao, S.-Z.; Shen, C.-B.; Ge, X.; Jiang, S.-Y. Nature and Evolution of the Ore-Forming Fluids from Nanmushu Carbonate-Hosted Zn-Pb Deposit in the Mayuan District, Shaanxi Province, Southwest China. *Geofluids* **2017**, *2017*, 2410504. [CrossRef]
20. Wang, H.; Wang, J.B.; Zhu, X.Y.; Cheng, X.Y.; Jiang, B.B. Discussion of ore-forming material source and sulfur and lead isotopic geochemistry of Mayuan Pb-Zn deposit in Shaanxi. *Miner. Resour. Geol.* **2017**, *31*, 241–247. (In Chinese with English Abstract)
21. Wang, G.; Huang, Z.; Zhao, F.; Li, N.; Fu, Y. The relationship between hydrocarbon accumulation and Mississippi Valley-type Pb-Zn mineralization of the Mayuan metallogenic belt, the northern Yangtze block, SW China: Evidence from ore geology and Rb-Sr isotopic dating. *Resour. Geol.* **2020**, *70*, 188–203. [CrossRef]
22. Song, Z.; Chen, C.; Yang, Y.; Zhang, Y.; Yin, L.; Li, H. Mineralization age and sources of ore-forming material of the Nanmushu Zn-Pb deposit in the Micangshan Tectonic Belt at the northern margin of the Yangtze Craton, China: Constraints from Rb-Sr dating and Sr-Pb isotopes. *Resour. Geol.* **2020**, *70*, 273–295. [CrossRef]
23. Li, H.M.; Chen, Y.C.; Wang, D.H.; Li, H.Q. Geochemistry and mineralization age of the Mayuan zinc deposit, Nanzheng, southern Shaanxi, China. *Geol. Bull. China* **2007**, *26*, 546–552. (In Chinese with English Abstract)
24. Hou, M.T. The relationship between organic matter and lead-zinc mineralization in the Mayuan lead-zinc deposit, Shaanxi Province. *Geol. China* **2009**, *36*, 861–870. (In Chinese with English Abstract)
25. Huang, Z.; Wang, G.; Li, N.; Fu, Y.; Lei, Q.; Mao, X. Genetic link between Mississippi Valley-Type (MVT) Zn-Pb mineralization and hydrocarbon accumulation in the Nanmushu, northern margin of Sichuan Basin, SW China. *Geochemistry* **2021**, *81*, 125805. [CrossRef]
26. Gao, Y.B.; Li, K.; Zhang, J.W.; Guo, W.; Han, Y.X.; Liu, T.H.; Chao, Y.Y. Geochemical characteristics of organic matters and metallogenesis of Mayuan Pb-Zn deposit in the northern margin of Yangtze Plate, China. *J. Earch Sci. Environ.* **2021**, *43*, 276–290. (In Chinese with English Abstract)
27. Chen, B.Y. Study on Geological Characteristics of Pb-Zn Deposits in Mayuan, Nanzheng County. Master's Thesis, Chang'an University, Xi'an, China, 2013. (In Chinese with English Abstract)
28. Qi, W.; Hou, M.T.; Wang, K.M.; Wang, D.G. A large-scale stratabound lead-zinc metallogenic belt discovered in the Mayuan area. *Geol. Bull. China* **2004**, *23*, 1139–1142. (In Chinese with English Abstract)
29. Li, H.M.; Wang, D.H.; Zhang, C.Q.; Chen, Y.C.; Li, L.X. Characteristics of trace and rare earth elements in minerals from some typical lead-zinc deposits of Shaanxi Province. *Miner. Depos.* **2009**, *28*, 434–448. (In Chinese with English Abstract)
30. Hu, P.; Wu, Y.; Zhang, C.Q.; Hu, M.Y. Trace and minor elements in sphalerite from the Mayuan lead-zinc deposit, northern margin of the Yangtze Plate: Implications from LA-ICP-MS analysis. *Acta Miner. Sin.* **2014**, *34*, 461–468. (In Chinese with English Abstract)
31. Wu, Y.; Kong, Z.G.; Chen, M.H.; Zhang, C.Q.; Cao, L.; Tang, Y.J.; Yuan, X.; Zhang, P. Trace elements in sphalerites from the Mississippi Valley-type lead-zinc deposits around the margins of Yangtze Block and its geological implications: A LA-ICPMS study. *Acta Petrol. Sin.* **2019**, *35*, 3443–3460. (In Chinese with English Abstract)
32. Liu, S.W.; Li, R.X.; Liu, Y.H.; Zeng, R. Geochemical characteristics and metallogenic mechanism of the Mayuan Pb-Zn deposit on the northern margin of Yangtze Plate. *Acta Geosci. Sin.* **2016**, *37*, 101–110. (In Chinese with English Abstract)
33. Song, Z.J.; Chen, C.H.; Zhang, Y.; Yin, L.; Li, H.Z.; Huang, X.D. Metallogenic sources of Nanmushu Pb-Zn deposit in Mayuan area, Shaanxi Province: Constraint from hydrogen and oxygen isotopes and trace elements. *Miner. Depos.* **2018**, *37*, 985–1000. (In Chinese with English Abstract)
34. Han, Y.X.; Liu, Y.H.; Liu, S.W.; Lei, W.S.; Li, Z.; Li, Y.T.; Li, X. Origin of the breccia and metallogenic geological background of Mayuan Pb-Zn deposit. *Earth Sci. Front.* **2016**, *23*, 94–101. (In Chinese with English Abstract)
35. Hou, M.T.; Wang, D.G.; Yang, Z.R.; Gao, J. Geological characteristics of lead-zinc mineralized zones in the Mayuan area, Shaanxi, and their ore prospects. *Geol. China* **2007**, *34*, 101–109. (In Chinese with English Abstract)
36. Paton, C.; Hellstrom, J.; Paul, B.; Woodhead, J.; Hergt, J. Iolite: Freeware for the visualisation and processing of mass spectrometric data. *J. Anal. Atom. Spectrom.* **2011**, *26*, 2508. [CrossRef]
37. Wilson, S.A.; Ridley, I.; Koenig, A.E. Development of sulfide calibration standards for the laser ablation inductively-coupled plasma mass spectrometry technique. *J. Anal. Atom. Spectrom.* **2002**, *17*, 406–409. [CrossRef]
38. Han, R.; Qin, K.; Groves, D.I.; Hui, K.; Li, Z.; Zou, X.; Li, G.; Su, S. Ore-formation at the Halasheng Ag-Pb-Zn deposit, northeast Inner Mongolia as revealed by trace-element and sulfur isotope compositions of ore-related sulfides. *Ore Geol. Rev.* **2022**, *144*, 104853. [CrossRef]

39. Erlandsson, V.B.; Wallner, D.; Ellmies, R.; Raith, J.G.; Melcher, F. Trace element composition of base metal sulfides from the sediment-hosted Dolostone Ore Formation (DOF) CuCo deposit in northwestern Namibia: Implications for ore genesis. *J. Geochem. Explor.* **2022**, *243*, 107105. [CrossRef]
40. Belissont, R.; Boiron, M.; Luais, B.; Cathelineau, M. LA-ICP-MS analyses of minor and trace elements and bulk Ge isotopes in zoned Ge-rich sphalerites from the Noailhac—Saint-Salvy deposit (France): Insights into incorporation mechanisms and ore deposition processes. *Geochim. Cosmochim. Acta* **2014**, *126*, 518–540. [CrossRef]
41. Liu, S.; Zhang, Y.; Ai, G.; Xue, X.; Li, H.; Shah, S.A.; Wang, N.; Chen, X. LA-ICP-MS trace element geochemistry of sphalerite: Metallogenic constraints on the Qingshuitang Pb–Zn deposit in the Qinhang Ore Belt, South China. *Ore Geol. Rev.* **2022**, *141*, 104659. [CrossRef]
42. Yang, Q.; Zhang, X.; Ulrich, T.; Zhang, J.; Wang, J. Trace element compositions of sulfides from Pb-Zn deposits in the Northeast Yunnan and northwest Guizhou Provinces, SW China: Insights from LA-ICP-MS analyses of sphalerite and pyrite. *Ore Geol. Rev.* **2022**, *141*, 104639. [CrossRef]
43. Oyebamiji, A.; Hu, R.; Zhao, C.; Zafar, T. Origin of the Triassic Qilinchang Pb-Zn deposit in the western Yangtze block, SW China: Insights from in-situ trace elemental compositions of base metal sulphides. *J. Asian Earth Sci.* **2020**, *192*, 104292. [CrossRef]
44. Zhou, J.; Yang, Z.; An, Y.; Luo, K.; Liu, C.; Ju, Y. An evolving MVT hydrothermal system: Insights from the Niujiaotang Cd-Zn ore field, SW China. *J. Asian Earth Sci.* **2022**, *237*, 105357. [CrossRef]
45. Luo, K.; Zhou, J.X.; Xu, C.; He, K.J.; Wang, Y.B.; Sun, G.T. The characteristics of the extraordinary germanium enrichment in the Wusihe large-scale Ge-Pb-Zn deposit, Sichuan Province, China and its geological significance. *Acta Petrol. Sin.* **2021**, *37*, 2761–2777. (In Chinese with English Abstract)
46. Bonnet, J.; Cauzid, J.; Testemale, D.; Kieffer, I.; Proux, O.; Lecomte, A.; Bailly, L. Characterization of Germanium Speciation in Sphalerite (ZnS) from Central and Eastern Tennessee, USA, by X-ray Absorption Spectroscopy. *Minerals* **2017**, *7*, 79. [CrossRef]
47. Johan, Z. Indium and germanium in the structure of sphalerite: An example of coupled substitution with copper. *Miner. Petrol.* **1988**, *39*, 211–229. [CrossRef]
48. Hu, Y.S.; Ye, L.; Huang, Z.L.; Li, Z.L.; Wei, C.; Danyushevskiy, L. Distribution and existing forms of trace elements from Maliping Pb-Zn deposit in northeastern Yunnan, China: A LA-ICPMS study. *Acta Petrol. Sin.* **2019**, *35*, 3477–3495. (In Chinese with English Abstract)
49. Wei, C.; Ye, L.; Hu, Y.; Huang, Z.; Danyushevsky, L.; Wang, H. LA-ICP-MS analyses of trace elements in base metal sulfides from carbonate-hosted Zn-Pb deposits, South China: A case study of the Maoping deposit. *Ore Geol. Rev.* **2021**, *130*, 103945. [CrossRef]
50. Yuan, B.; Zhang, C.; Yu, H.; Yang, Y.; Zhao, Y.; Zhu, C.; Ding, Q.; Zhou, Y.; Yang, J.; Xu, Y. Element enrichment characteristics: Insights from element geochemistry of sphalerite in Daliangzi Pb–Zn deposit, Sichuan, Southwest China. *J. Geochem. Explor.* **2018**, *186*, 187–201. [CrossRef]
51. Ye, L.; Li, Z.L.; Hu, Y.S.; Huang, Z.L.; Zhou, J.X.; Fan, H.F.; Danyushevskiy, L. Trace elements in sulfide from the Tianbaoshan Pb-Zn deposit, Sichuan Province, China: A LA-ICPMS study. *Acta Petrol. Sin.* **2016**, *32*, 3377–3393. (In Chinese with English Abstract)
52. Zhou, J.X.; Yang, D.Z.; Yu, J.; Luo, K.; Zhou, Z.H. Ge extremely enriched in the Zhulingou Zn deposit, Guiding City, Guizhou Province, China. *Geol. China* **2021**, *48*, 665–666. (In Chinese with English Abstract)
53. Hu, Y.; Wei, C.; Ye, L.; Huang, Z.; Danyushevsky, L.; Wang, H. LA-ICP-MS sphalerite and galena trace element chemistry and mineralization-style fingerprinting for carbonate-hosted Pb-Zn deposits: Perspective from early Devonian Huodehong deposit in Yunnan, South China. *Ore Geol. Rev.* **2021**, *136*, 104253. [CrossRef]
54. Cook, N.J.; Ciobanu, C.L.; Brugger, J.; Etschmann, B.; Howard, D.L.; Jonge, M.D.D.; Ryan, C.; Paterson, D. Determination of the oxidation state of Cu in substituted Cu-In-Fe-bearing sphalerite μ-XANES spectroscopy. *Am. Miner.* **2011**, *97*, 476–479. [CrossRef]
55. Belissont, R.; Muñoz, M.; Boiron, M.; Luais, B.; Mathon, O. Distribution and oxidation state of Ge, Cu and Fe in sphalerite by μ-XRF and K-edge μ-XANES: Insights into Ge incorporation, partitioning and isotopic fractionation. *Geochim. Cosmochim. Acta* **2016**, *177*, 298–314. [CrossRef]
56. Liu, W.; Mei, Y.; Etschmann, B.; Glenn, M.; Macrae, C.M.; Spinks, S.C.; Ryan, C.G.; Brugger, J.; Paterson, D.J. Germanium speciation in experimental and natural sphalerite: Implications for critical metal enrichment in hydrothermal Zn-Pb ores. *Geochim. Cosmochim. Acta* **2023**, *342*, 198–214. [CrossRef]
57. Fan, M.; Ni, P.; Pan, J.; Wang, G.; Ding, J.; Chu, S.; Li, W.; Huang, W.; Zhu, R.; Chi, Z. Rare disperse elements in epithermal deposit: Insights from LA–ICP–MS study of sphalerite at Dalingkou, South China. *J. Geochem. Explor.* **2023**, *244*, 107124. [CrossRef]
58. Pring, A.; Wade, B.; Mcfadden, A.; Lenehan, C.E.; Cook, N.J. Coupled Substitutions of Minor and Trace Elements in Co-Existing Sphalerite and Wurtzite. *Minerals* **2020**, *10*, 147. [CrossRef]
59. Guo, F.; Wang, Z.L.; Xu, D.R.; Yu, D.S.; Dong, G.J.; Ning, J.T.; Kang, B.; Peng, E.K. Trace element characteristics of sphalerite in the Lishan Pb-Zn-Cu polymetallic deposit in Hunan Province and the metallogenic implications. *Earth Sci. Front.* **2020**, *27*, 66–81. (In Chinese with English Abstract)
60. Ye, L.; Gao, W.; Yang, Y.L.; Liu, T.G.; Peng, S.S. Trace elements in sphalerite in Laochang Pb-Zn polymetallic deposit, Lancang, Yunnan Province. *Acta Petrol. Sin.* **2012**, *28*, 1362–1372. (In Chinese with English Abstract)
61. Oyebamiji, A.; Falae, P.; Zafar, T.; Rehman, H.U.; Oguntuase, M. Genesis of the Qilinchang Pb–Zn deposit, southwestern China: Evidence from mineralogy, trace elements systematics and S–Pb isotopic characteristics of sphalerite. *Appl. Geochem.* **2023**, *148*, 105545. [CrossRef]

62. Shen, H.; Zhang, Y.; Zuo, C.; Shao, Y.; Zhao, L.; Lei, J.; Shi, G.; Han, R.; Zheng, X. Ore-forming process revealed by sphalerite texture and geochemistry: A case study at the Kangjiawan Pb–Zn deposit in Qin-Hang Metallogenic Belt, South China. *Ore Geol. Rev.* **2022**, *150*, 105153. [CrossRef]
63. Knorsch, M.; Nadoll, P.; Klemd, R. Trace elements and textures of hydrothermal sphalerite and pyrite in Upper Permian (Zechstein) carbonates of the North German Basin. *J. Geochem. Explor.* **2020**, *209*, 106416. [CrossRef]
64. Li, X.; Zhang, Y.; Li, Z.; Zhao, X.; Zuo, R.; Xiao, F.; Zheng, Y. Discrimination of Pb-Zn deposit types using sphalerite geochemistry: New insights from machine learning algorithm. *Geosci. Front.* **2023**, *14*, 101580. [CrossRef]
65. Bauer, M.E.; Burisch, M.; Ostendorf, J.; Krause, J.; Frenzel, M.; Seifert, T.; Gutzmer, J. Trace element geochemistry of sphalerite in contrasting hydrothermal fluid systems of the Freiberg district, Germany: Insights from LA-ICP-MS analysis, near-infrared light microthermometry of sphalerite-hosted fluid inclusions, and sulfur isotope geochemistry. *Miner. Depos.* **2019**, *54*, 237–262.
66. Frenzel, M.; Cook, N.J.; Ciobanu, C.L.; Slattery, A.D.; Wade, B.P.; Gilbert, S.; Ehrig, K.; Burisch, M.; Verdugo-ihl, M.R.; Voudouris, P. Halogens in hydrothermal sphalerite record origin of ore-forming fluids. *Geology* **2020**, *48*, 766–770. [CrossRef]
67. Lee, J.H.; Yoo, B.C.; Yang, Y.; Lee, T.H.; Seo, J.H. Sphalerite geochemistry of the Zn-Pb orebodies in the Taebaeksan metallogenic province, Korea. *Ore Geol. Rev.* **2019**, *107*, 1046–1067. [CrossRef]
68. Fan, X.; Lü, X.; Wang, X. Textural, chemical, isotopic and microthermometric features of sphalerite from the Wunuer deposit, Inner Mongolia: Implications for two stages of mineralization from hydrothermal to epithermal. *Geol. J.* **2020**, *55*, 6936–6958. [CrossRef]
69. Sun, G.; Zeng, Q.; Zhou, J.; Zhou, L.; Chen, P. Genesis of the Xinling vein-type Ag-Pb-Zn deposit, Liaodong Peninsula, China: Evidence from texture, composition and in situ S-Pb isotopes. *Ore Geol. Rev.* **2021**, *133*, 104120. [CrossRef]
70. Benites, D.; Torró, L.; Vallance, J.; Laurent, O.; Valverde, P.E.; Kouzmanov, K.; Chelle-michou, C.; Fontboté, L. Distribution of indium, germanium, gallium and other minor and trace elements in polymetallic ores from a porphyry system: The Morococha district, Peru. *Ore Geol. Rev.* **2021**, *136*, 104236. [CrossRef]
71. Chu, X.; Li, B.; Shen, P.; Zha, Z.; Lei, Z.; Wang, X.; Tao, S.; Hu, Q. Trace elements in sulfide minerals from the Huangshaping copper-polymetallic deposit, Hunan, China: Ore genesis and element occurrence. *Ore Geol. Rev.* **2022**, *144*, 104867. [CrossRef]
72. Zhuang, L.; Song, Y.; Liu, Y.; Fard, M.; Hou, Z. Major and trace elements and sulfur isotopes in two stages of sphalerite from the world-class Angouran Zn–Pb deposit, Iran: Implications for mineralization conditions and type. *Ore Geol. Rev.* **2019**, *109*, 184–200. [CrossRef]
73. Liu, Y.; Qi, H.; Bi, X.; Hu, R.; Qi, L.; Yin, R.; Tang, Y. Two types of sediment-hosted Pb-Zn deposits in the northern margin of Lanping basin, SW China: Evidence from sphalerite trace elements, carbonate C-O isotopes and molybdenite Re-Os age. *Ore Geol. Rev.* **2021**, *131*, 104016. [CrossRef]
74. Wei, C.; Ye, L.; Huang, Z.; Hu, Y.; Wang, H. In situ trace elements and S isotope systematics for growth zoning in sphalerite from MVT deposits: A case study of Nayongzhi, South China. *Min. Mag.* **2021**, *85*, 364–378. [CrossRef]
75. Cugerone, A.; Cenki-tok, B.; Muñoz, M.; Kouzmanov, K.; Oliot, E.; Motto-ros, V.; Legoff, E. Behavior of critical metals in metamorphosed Pb-Zn ore deposits: Example from the Pyrenean Axial Zone. *Miner. Depos.* **2021**, *56*, 685–705. [CrossRef]
76. Cave, B.; Lilly, R.; Barovich, K. Textural and geochemical analysis of chalcopyrite, galena and sphalerite across the Mount Isa Cu to Pb-Zn transition: Implications for a zoned Cu-Pb-Zn system. *Ore Geol. Rev.* **2020**, *124*, 103647. [CrossRef]
77. Cave, B.; Lilly, R.; Hong, W. The Effect of Co-Crystallising Sulphides and Precipitation Mechanisms on Sphalerite Geochemistry: A Case Study from the Hilton Zn-Pb (Ag) Deposit. *Aust. Miner.* **2020**, *10*, 797. [CrossRef]
78. Cave, B.; Perkins, W.; Lilly, R. Linking uplift and mineralisation at the Mount Novit Zn-Pb-Ag Deposit, Northern Australia: Evidence from geology, U–Pb geochronology and sphalerite geochemistry. *Geosci. Front.* **2022**, *13*, 101347. [CrossRef]
79. Maurer, M.; Prelević, D.; Mertz-kraus, R.; Pačevski, A.; Kostić, B.; Malbašić, J. Genesis and metallogenetic setting of the polymetallic barite-sulphide deposit, Bobija, Western Serbia. *Int. J. Earth Sci.* **2019**, *108*, 1725–1740. [CrossRef]
80. Zhao, Y.; Chen, S.; Tian, H.; Zhao, J.; Tong, X.; Chen, X. Trace element and S isotope characterization of sulfides from skarn Cu ore in the Laochang Sn-Cu deposit, Gejiu district, Yunnan, China: Implications for the ore-forming process. *Ore Geol. Rev.* **2021**, *134*, 104155. [CrossRef]
81. Xiong, Y.; Zhou, T.; Fan, Y.; Chen, J.; Wang, B.; Liu, J.; Wang, F. Enrichment mechanisms and occurrence regularity of critical minerals resources in the Yaojialing Zn skarn polymetallic deposit, Tongling district, eastern China. *Ore Geol. Rev.* **2022**, *144*, 104822. [CrossRef]
82. Xing, B.; Mao, J.; Xiao, X.; Liu, H.; Jia, F.; Wang, S.; Huang, W.; Li, H. Genetic discrimination of the Dingjiashan Pb-Zn deposit, SE China, based on sphalerite chemistry. *Ore Geol. Rev.* **2021**, *135*, 104212. [CrossRef]
83. Lu, S.; Ren, Y.; Yang, Q.; Sun, Z.; Hao, Y.; Sun, X. Ore Genesis for Stratiform Ore Bodies of the Dongfengnanshan Copper Polymetallic Deposit in the Yanbian Area, NE China: Constraints from LA-ICP-MS in situ Trace Elements and Sulfide S–Pb Isotopes. *Acta Geol. Sin.* **2019**, *93*, 1591–1606. [CrossRef]
84. Torró, L.; Benites, D.; Vallance, J.; Laurent, O.; Ortiz-benavente, B.A.; Chelle-michou, C.; Proenza, J.A.; Fontboté, L. Trace element geochemistry of sphalerite and chalcopyrite in arc-hosted VMS deposits. *J. Geochem. Explor.* **2022**, *232*, 106882. [CrossRef]
85. Zhang, Q. Application of diagram of trace elements in the sphalerite and galena to the genetic type of lead and zinc deposit. *Geol. Geochem* **1987**, 64–66. (In Chinese with English Abstract)
86. Zhou, J.; Huang, Z.; Zhou, G.; Li, X.; Ding, W.; Bao, G. Trace Elements and Rare Earth Elements of Sulfide Minerals in the Tianqiao Pb-Zn Ore Deposit, Guizhou Province, China. *Acta Geol. Sin.* **2011**, *85*, 189–199.

87. Zhu, L.M.; Yuan, H.H.; Luan, S.W. Typomorphic characteristics and their significance of minor elements of sphalerite from Disu and Daliangzi Pb-Zn deposits, Sichuan. *Acta Geol. Sichuan* **1995**, *15*, 49–55. (In Chinese with English Abstract)
88. Li, Z.L.; Ye, L.; Huang, Z.L.; Nian, H.L.; Zhou, J.X. Primary research on trace elements in sphalerite from Tianqiao Pb-Zn deposit, northwestern Guizhou Province, China. *Acta Miner. Sin* **2016**, *36*, 183–188. (In Chinese with English Abstract)
89. Chen, C.H.; Song, Z.J.; Yang, Y.L.; Yang, D.P.; Gu, Y.; Chen, X.J. Characteristics of trace elements of sphalerite and genesis of the Dongzigou lead-zinc deposit in Xishui County, Guizhou Province, China. *Acta Miner. Sin.* **2019**, *39*, 485–493. (In Chinese with English Abstract)
90. Leach, D.L.; Bradley, D.; Lewchuk, M.T.; Symons, D.T.; Marsily, G.D.; Brannon, J. Mississippi Valley-type lead–zinc deposits through geological time: Implications from recent age-dating research. *Miner. Depos.* **2001**, *36*, 711–740. [CrossRef]
91. Leach, D.; Sangster, D.; Kelley, K.; Large, R.; Garven, G.; Allen, C.; Gutzmer, J.; Walters, S. Sediment-hosted lead-zinc deposits: A global perspective. *Econ. Geol.* **2005**, *100th Anniversary Volume*, 561–607.